

Versatile NMR simulations using SIMPSON

Dennis W. Juhl^{a,b}, Zdeněk Tošner^c, Thomas Vosegaard^{a,b}

^aDepartment of Chemistry, Aarhus University, Aarhus, Denmark

^bInterdisciplinary Nanoscience Center (iNANO), Aarhus University, Aarhus, Denmark

^cDepartment of Chemistry, Faculty of Science, Charles University, Prague, Czech Republic

Contents

1. Introduction	2
2. Basic concepts	3
2.1 Elements of the SIMPSON input file	4
2.2 Theory overview	9
3. Basic SIMPSON examples	12
3.1 CSA static and MAS	12
3.2 ¹ H decoupling	16
3.3 Cross-polarization	19
3.4 REDOR	21
3.5 Fitting an experimental spectrum	26
3.6 Satellite transitions for quadrupolar nuclei	28
3.7 Second-order quadrupolar line shapes	31
3.8 RF pulses for quadrupolar nuclei	33
3.9 Triple-quantum coherence excitation in MQMAS experiments	34
4. SIMMOL	35
4.1 Establishment of a spin system	36
5. NMR simulations of proteins and peptides	40
5.1 PISA wheels	40
5.2 Ultrafast magic-angle spinning	41
5.3 NCOCA solid-state NMR optimization	44
6. Optimal control	47
7. Dynamics	50
8. Conclusions	54
Acknowledgements	55
References	55

Abstract

This chapter provides a number of examples of numerical simulations in NMR. Main focus is on advanced simulations in solid-state NMR using the widely used SIMPSON simulation package. The chapter starts with introductory examples providing a gentle

introduction to SIMPSON and various concepts of solid-state NMR. Following the introduction is a demonstration on how SIMPSON can interact with SIMMOL for setting up spin systems of protein spin systems. Finally, we demonstrate how the versatile Tcl interface of SIMPSON can be used to expand the capabilities of SIMPSON, here exemplified by simulations of chemical exchange. The examples demonstrate that SIMPSON may be regarded a 'virtual NMR spectrometer'.

Keywords: Solid-state NMR, Numerical simulations, SIMPSON, Virtual spectrometer



1. Introduction

Since the early days of NMR, researchers have benefitted from the precise relation between the response of the nuclear spins in the spectrometer and the theoretical descriptions of NMR [1–5]. This holds both for liquid-state NMR pulse sequences, where the product-operator formalism is very effective [2], for solids where anisotropic interactions need be considered [3], and for relaxation in liquids [4,5]. In many cases, it is not possible to derive analytical solutions, in which case researchers turn to numerical simulations. Such examples include (i) pulse sequences, where effects of finite radio-frequency (rf) pulses (nuclear spin interactions occurring simultaneously with the rf pulses) cannot be neglected, (ii) powder patterns in solids, where the analytical description of the line shape cannot be derived, and (iii) when fitting experimental line shapes.

The nuclear spin interactions that are measured in NMR experiments of solid samples carry important information on the molecular structure and dynamics. The most obvious example is the dipole-dipole interaction between two nuclei, which is inversely proportional to the internuclear distance to the third power. The chemical shift may also be related to structure, either through empirically established relations or by comparison with quantum-chemical calculations. Finally, the quadrupole coupling and J-coupling interactions are sensitive reporters on various molecular features. As such, the nuclear spin interactions are equivalent to electron density maps that crystallographers use to determine crystal structures by X-ray diffraction.

The nuclear spin interactions are measured experimentally through line shapes and eventually complex pulse sequences. In the past decades, substantial efforts have been put into the development of NMR experiments that measure the magnitude of the different nuclear spin interactions with high precision. The development of such pulse sequences has led to many

recent breakthroughs in solid-state NMR in so diverse areas as determining atomic-resolution structures of membrane proteins [6–8] and fibrillating proteins [9–11], structural characterization of functional materials [12], and NMR crystallography [13] to name a few. Common for all of these studies, and most other solid-state NMR studies in the literature, is that they rely heavily on advanced numerical simulations to extract the structural information from the NMR data.

Previously, most solid-state NMR research groups developed in-house software solutions for their specific needs for numerical simulations as part of the interpretation of their data. This severely limited the exchange of knowledge and competences in the community. Later, substantial efforts have been devoted to the development of software for numerical simulations in solid-state NMR [14–21], which can be divided into two different classes: (i) User-friendly software for fitting experimental spectra [14,15,17,18], and (ii) software to understand the underlying spin dynamics [16,19–23]. The first class is generally easy to use and can be used without much prior knowledge. The second class is more versatile but generally is associated with a steeper learning curve.

This chapter is written for students and researchers new to numerical simulations in solid-state NMR as well as for more experienced users of the versatile simulation program SIMPSON. The aim is to demonstrate a number of simulations in different areas of solid-state NMR ranging from basic introductory examples to advanced simulations of complex pulse sequences or spin systems. This program was developed to simulate any spin system and any pulse sequence. The applications presented here will illustrate this by including basic introductory simulations that demonstrate the concept of anisotropic interactions, powder averaging, nuclear spin interactions, etc. and more advanced simulations including pulse-sequence optimization and fitting experimental spectra. More advanced examples for simulations of biological solid-state NMR experiments will also be presented.



2. Basic concepts

SIMPSON is very versatile and may be regarded as a virtual spectrometer able to simulate any spin system under various experimental conditions. To achieve this flexibility, all relevant parameters obviously need to be defined to be included in the simulations. SIMPSON reads its instructions

from an input file, written in a scripting language. SIMPSON is based on the Tool Command Language (Tcl) [24], which is a very flexible and widely community-supported scripting language. Since SIMPSON interprets the Tcl input file, it may be considered an advanced Tcl interpreter that has been extended with instructions for spin systems, pulse sequences, and spectrum processing features. This also means that all functionality of Tcl is available in SIMPSON including the possibility to load third-party libraries. The advantage of relying on a well-established scripting language is that many libraries have been developed for completely different purposes and that extensive documentation is available online (see e.g. Ref [24]).

2.1 Elements of the SIMPSON input file

A typical SIMPSON input file contains four sections

1. A specification of the spin system (the virtual sample): `spinsys { ... }`
2. A specification of elements of the virtual spectrometer: `par { ... }`
3. A specification of the pulse sequence: `proc pulseq { ... }`
4. A section to control the simulation: `proc main { ... }`

The spin system section is defined by the instruction `spinsys {...}` which defines the size of the spin system (number and type of nuclei) and specifies each of the nuclear spin interactions. The nuclear spin interactions may include chemical shifts, J-couplings, dipole-dipole couplings, and quadrupole coupling tensorial interactions. For the dipole-dipole coupling, it is possible to specify a motionally averaged dipolar interaction (`dipolar_ave`), which appears as a dipolar interaction with an asymmetry parameter.

A simple example of a spin system involving a single ^1H nucleus with an isotropic chemical shift of 5 ppm and a chemical shift anisotropy of 10 ppm for with an asymmetry parameter of $\eta=0.5$ may be specified as.

```
spinsys {  
  channels 1H  
  nuclei 1H  
  shift 1 5p 10p 0.5 0 0 0  
}
```

The Tcl code `spinsys {...}` invokes a call to the built-in procedure ‘`spinsys`’, which sets up the spin system with the given parameters. The first line defines the channels used in the experiments. Like at the spectrometer, all isotopes in the experiment must be connected to a channel. Next, all nuclei in the sample are defined. If, for instance, two different hydrogen atoms were present in the sample, they should be listed as two nuclei:

nuclei 1H 1H. If the experiment includes one carbon and two protons, the three nuclei would be listed.

```
channels 1H 13C
nuclei 1H 1H 13C
```

After defining the nuclei involved, all the relevant spin interactions should be defined. In the example above, only the chemical shift is specified, by the seven numbers following the shift command: (1) The nucleus number (the nuclei specified range from 1 to N, where N is the total number of nuclei), (2) the isotropic chemical shift given in Hz by default, but by appending a “p” as above, the number will be interpreted as ppm, (3) the chemical shift anisotropy (see Ref. [16] for a definition), (4) the asymmetry parameter (η), (5–7) three Euler angles specifying the orientation of the shift tensor in the crystal reference frame (see definition of reference frames below). Fig. 1 gives a complete list of nuclear spin interactions implemented in SIMPSON and the parameters to define them.

```

shift 1 100 500 0.2 -18 90 120
      ①      ②      ③

quadrupole 1 2 3e6 0.2 -18 90 120
           ① ④      ②      ③

dipole 1 2 -1000 0 90 45
       ① ②      ③

jcoupling 1 2 120 -50 0.2 -18 90 120
          ① ②      ③

dipole_ave 1 2 1e3 0.2 -18 90 120
           ① ②      ③

```

Fig. 1 Overview of the different nuclear spin interactions available in SIMPSON. The spin number or spin-pair numbers (red) are marked (1), the magnitude of the tensor is marked (2), and the three Euler angles representing the orientation of the tensor marked (3). The magnitude of the tensor is represented by the isotropic value (chemical shift and J coupling) the anisotropic value (all interactions), and the asymmetry parameter (all but dipole–dipole interaction). For the quadrupole coupling interaction, the highest order of the interaction is given as (4). Only first and second-order interactions are available in SIMPSON. Interaction strengths are given in Hz, but for the chemical shift interaction, the isotropic and anisotropic values may be followed by a ‘p’ indicating that the value is given in ppm (see text).

The second section of the SIMPSON input file is the definition of all other parameters needed to set up the simulation. The complete list of possible instructions is given in Refs [16, 22, 23]. An example could be.

```

par {
  spin_rate      10000
  start_operator 11z
  detect_operator 12p
  proton_frequency 1.2e9
  np             512
  gamma_angles   8
  sw             gamma_angles*spin_rate
  crystal_file   rep320
  verbose        1101
  variable tsw   1.0e6/sw
  variable rf    50000
  variable t90   0.25e6/rf
}

```

This example demonstrates some of the possibilities including basic calculations and definition of variables. All quantities are specified without units, with the implicit requirement that frequencies are given in Hz (thus in the example above, the spin rate is $\nu_r = 10$ kHz, and the Larmor frequency for ^1H is $\omega_0/2\pi = 1.2$ GHz) and all pulses and delays are specified in μs . Hence, the user defined variable `tsw` corresponds to the dwell time in μs . The `verbose` entry takes up to eight zeroes or ones instructing SIMPSON to provide output about (i) the spin system, (ii) the simulation progress, (iii) simulation information, (iv) start and detect operators, (v) powder angles, (vi) the rf averaging profile, (vii) the acquisition block, and (viii) the averaging file. The above value 1101 asks SIMPSON to provide output about the spin system, the simulation progress, and the start- and detect operators.

The `crystal_file` entry controls the potential powder averaging and can specify either an internal or external crystal file that contains the (α, β) angle pairs for the powder averaging (see below). Internal options, for the crystal file are: `alpha0beta0`, `alpha0beta90`, `rep10`, `rep20`, `rep30`, `rep66`, `rep100`, `rep144`, `rep168`, `rep256`, `rep320`, `rep678`, `rep2000`, `zcw20`, `zcw33`, `zcw54`, `zcw88`, `zcw143`, `zcw232`, `zcw376`, `zcw615`, `zcw986`, `zcw4180`, and `zcw28656`. Crystal files `alpha0beta0` and `alpha0beta90` correspond to single crystallites with angles of $(\alpha, \beta) = (0^\circ, 0^\circ)$ and $(\alpha, \beta) = (0^\circ, 90^\circ)$, respectively. These crystallite files are used to mimic single-crystal or liquid samples. The `repXX` crystallites are

generated using the REPULSION algorithm [25] with XX crystallites, while the ZCWXX crystallites are generated using the approach of Zaremba [26], Conroy [27], and Wolfsberg [28]. In general, we find that REPULSION crystallites work best for smaller crystallite sets (fewer than some hundreds of crystallites), while ZCW crystallites work best for larger sets. Throughout this paper, we treat the γ averaging separately, since this angle needs not be averaged for static samples and may be averaged in synchrony with the time propagation in favourable cases with sample spinning. However, SIMPSON is able to handle crystallite files with all three Euler angles. In cases where this is preferred, substantial efforts have been invested in developing efficient three-angle sets [29,30], which may be readily embedded in SIMPSON as an external crystallite file.

The pulse sequence section of the SIMPSON input file is the definition of a Tcl procedure named `pulseseq`

```
proc pulseseq {} {
    global par

    pulse $par(t90) $par(rf) x
    acq_block {
        delay $par(tsw)
    }
}
```

The first statement `global par` is a Tcl instruction that makes the parameter named ‘par’ available in the procedure. If not specified, the program would complain that the parameter `$par(t90)` is undefined in the `pulseseq` procedure. Thereafter, a 90° pulse is used to flip the magnetization into the xy-plane, and acquisition is performed by the `acq_block` command of SIMPSON. With this command, the FID points are separated by the inverse of the spectral width corresponding to the normal dwell time, and the propagator is obtained using the instruction following the `acq_block` statement, in this case just a delay. Hence, the above pulse sequence corresponds to a normal single-pulse experiment.

The key elements of a pulse sequence are pulses, delays, offset and acquisition instructions, which may be setup in sequence by Tcl commands like for loops, etc. A `pulse` instruction takes a number of arguments. First is the length of the pulse (in μs), then followed by two arguments for each channel (defined in the `spinsys` section): `rf` amplitude (in Hz) and the phase of the pulse (in degrees or as `x`, `y`, `-x`, `-y`). A `delay` instruction takes only one argument: the duration (in μs). If you want to specify a pulse on one channel

simultaneously with a delay on another channel, the delay is implemented as a pulse with zero rf field strength. An `offset` instruction requires specification of the transmitter carrier offset in Hz for each channel. Finally, the `acq_block` instruction takes one argument, which is a list of pulses and delays.

Keeping the analogy to the virtual NMR spectrometer, the main section of the SIMPSON input file contains the instructions the operator of the spectrometer would normally give to the spectrometer computer including starting acquisition, apodization, Fourier Transforming, and saving the spectrum. In SIMPSON terminology, this is embedded in the Tcl procedure called `main`:

```
proc main {} {
    # make the par variables available in this procedure
    global par

    # perform the simulation and store the FID as variable f
    set f [fsimpson]
    # add 100 Hz line broadening to the FID stored in $f
    faddlb $f 100 0
    # zerofill the FID
    fzerofill $f 1024
    # perform a Fourier transformation
    fft $f
    # save the spectrum in SIMPSON's binary format
    fsave $f $par(name).spe -binary
}
```

In this example, we have used Tcl's possibility to make non-interpreted comments by starting lines with the hashtag character '#'. The 'experiment' is started by the command `fsimpson`, which starts the simulation and calculates the FID using the pulse sequence and other parameters specified in the input file. The command `fsimpson` returns a handle to the dataset, and the nomenclature `set f [...]` is the Tcl instruction for defining the variable `f` with the value returned by the function in the square brackets. The following lines perform apodization (add line broadening, `faddlb`), zerofilling, Fourier transformation, and saving the spectrum. All of these instructions operate on the dataset handle. Note that while the name of the variable storing the dataset handle is `f`, the value of the variable is obtained by the instruction `$f` in Tcl.

It can be noted that as part of a conventional Tcl input file, we may create other procedures to perform specific tasks. For example, in the examples prepared with this chapter, we have redefined the command `fsave` to allow saving SIMPSON data in the Core Scientific Data Model [31], which is more flexible than the default SIMPSON file format.

2.2 Theory overview

We will not go into details with the underlying theory of solid-state NMR in this chapter, but just summarize the essential parts necessary to understand the simulation environment. For further details see refs. [16, 22, 23].

The Hamiltonian describing our spin system in the Zeeman interaction frame takes the general form, in which all terms may be time dependent.

$$\widehat{H}(t) = \widehat{H}_{CS}(t) + \widehat{H}_{Dip}(t) + \widehat{H}_Q(t) + \widehat{H}_J(t) + \widehat{H}_{rf}(t) \quad (1)$$

referring to the tensorial chemical shift (CS), homo- and heteronuclear dipole-dipole coupling (Dip), quadrupolar (Q), J-coupling (J) nuclear spin interactions as well as the rf field (rf). Expressions for these Hamiltonians are given elsewhere [16]. This Hamiltonian directs the density operator according to the Liouville-von-Neumann equation.

$$\frac{d}{dt}\widehat{\rho}(t) = -i[\widehat{H}(t), \widehat{\rho}(t)]. \quad (2)$$

The solution to this differential equation introduces the propagator in the equation of motion.

$$\widehat{\rho}(t) = \widehat{U}(t)\widehat{\rho}(0)\widehat{U}^{-1}(t), \quad \widehat{U}(t) = \widehat{T}e^{-i\int_0^t\widehat{H}(t')dt'} \quad (3)$$

where \widehat{T} is the Dyson time-ordering operator that ensures correct evaluation of the integral that involves non-commuting terms.

SIMPSON establishes expressions of all terms of the Hamiltonian in Hilbert space, where the spin operators may be described by a square matrix of dimensions $(2I+1) \times (2I+1)$, where I is the nuclear spin quantum number of the nucleus. When the spin system contains more nuclei, the Hilbert-space matrices are expanded through the tensor product of the matrices for the individual spins, leading to overall matrix dimensions $n \times n$ of a spin system with N spins, where n is given by.

$$n = \prod_{i=1}^N (2I_i + 1). \quad (4)$$

Thus, a spin system with 10 ^1H atoms (spin $I=1/2$) has matrix dimensions of $2^{10} \times 2^{10} = 1024 \times 1024$, and a spin system consisting of two ^{93}Nb atoms (spin $I=9/2$) has dimensions $10^2 \times 10^2 = 100 \times 100$. Due to the exponential growth of matrix dimensions with the number of spins, selecting a small yet relevant spin system is crucial. Most of the internal computations

involve matrix multiplication and diagonalization, which both are operations where the computation time scales with the matrix dimensions in the third power. Hence, adding an additional hydrogen atom to the simulation will in general make the computation eight times longer.

SIMPSON solves the equation of motion (Eq. (3)) by dividing the pulse sequence into sufficiently small steps that the Hamiltonian may be considered time-independent over the time step and then finds the most efficient way to calculate the overall propagator [23]. In favourable cases, SIMPSON exploits the potential sparsity of the matrices through arranging the Hamiltonian in a block-diagonal fashion, leading to significant reduction of the computation time. Knowing the propagator, the specified start operator $\widehat{\rho}(0)$ in Eq. ((3)) is propagated to find $\widehat{\rho}(t)$ and its projection onto the detect operator \widehat{Q}_{det} to give the detected signal.

$$s(t) = \left\langle \widehat{Q}_{\text{det}}^\dagger | \widehat{\rho}(t) \right\rangle. \quad (5)$$

When this equation is evaluated in matrix formalism, we calculate $s(t) = \text{Tr}\left(\widehat{Q}_{\text{det}}\widehat{\rho}(t)\right)$. The result scales with the size of the matrix, so a two-spin system will have a different scaling than a single-spin system. It would be possible to scale internally, but which scaling should be chosen is not obvious. Hence, we have chosen to provide the signal unscaled in SIMPSON.

The Hamiltonians for the nuclear spin interactions may conveniently be written in the irreducible spherical tensor formalism, where they in general consist of a rank-0 and a rank-2 term, and for the second-order quadrupolar interaction also a rank-4 term.

$$\widehat{H}_\lambda = \sum_{l=0,2,(4)} (A_{l0}^\lambda)^L \widehat{T}_{l0}^\lambda \quad (6)$$

where $(A_{l0}^\lambda)^L$ is the spatial rank- l element of interaction λ expressed in the laboratory (L) frame, and \widehat{T}_{l0}^λ is the spin-part of the Hamiltonian.

The spatial part of the Hamiltonian is established through the magnitude and asymmetry of the tensor and the orientation of its principal axis frame in the crystal frame. The orientation is specified by three Euler angles using the convention shown in Fig. 2A. Commonly, we represent the coordinate transformation from frame X to frame Y by the Euler angles $\Omega_{XY} = (\alpha_{XY}, \beta_{XY}, \gamma_{XY})$. To obtain the description of the tensor in the laboratory frame, we use a series of coordinate transformations as outlined in Fig. 2B.

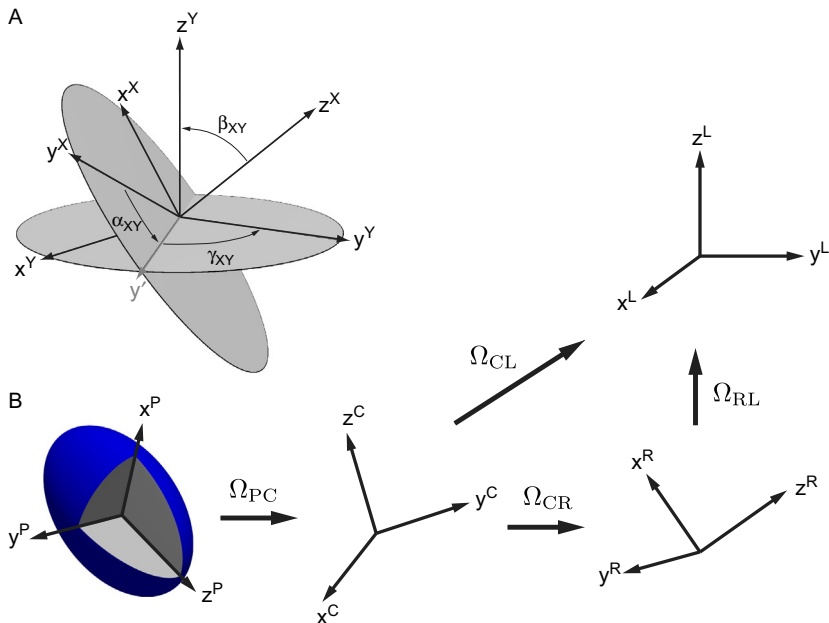


Fig. 2 (A) Illustration of the rotations performed with three Euler angles relating two frames marked X and Y. (B) Coordinate transformations used in SIMPSON. The nuclear spin interactions are defined in their principal axis frame 'P', then transformed into the crystal frame 'C' using the Euler angles Ω_{PC} , then for static samples transformed directly into the laboratory frame 'L' through Ω_{CL} . For spinning samples, the intermediate rotor frame 'R' is required.

Note the difference between the static and MAS case, since we need to include a rotor-fixed coordinate system to simulate the effect of MAS.

In the static case, the second-rank tensor transforms as.

$$(A_{20}^{\lambda})^L = \lambda_{\text{aniso}} \left(\frac{(3 \cos^2 \beta_{PL} - 1)}{2} - \eta \sqrt{\frac{3}{8}} \cos 2\alpha_{PL} \sin^2 \beta_{PL} \right), \quad (7)$$

with Ω_{PL} representing the Euler angles for the rotation $P \rightarrow L$.

The powder averaging is performed by the coordinate transformation relating the crystal frame to either the laboratory frame or the rotor frame, i.e. through Ω_{CL} or Ω_{CR} . The first case applies to static samples, for which the last Euler angle γ_{CL} corresponding to a rotation around the z axis in the laboratory frame is irrelevant, hence only the two angles α_{CL} , β_{CL} are necessary. For a spinning sample, the axis of the last rotation coincides with the rotor axis, hence all time-dependent terms of the Hamiltonian include $\omega_R t + \gamma_{CR}$, why we have chosen to keep the γ -angle of the crystallite

averaging separate in both the static and MAS case, as in many cases we can make an efficient propagation e.g. using the γ -COMPUTE algorithm [32]. Summation over different α_{CL} , β_{CL} crystallites in SIMPSON is done by providing a so-called crystal file that contains a list of crystallites and their relative weights. SIMPSON has a number of built-in crystal files as listed above.



3. Basic SIMPSON examples

The following section provides a number of basic SIMPSON examples that we have used at summer schools, courses, and at conferences. The examples have a dual purpose in this context: (i) Introducing the features of the SIMPSON simulation environment and (ii) providing an introduction to basic concepts of solid-state NMR such as powder averaging, magic-angle spinning, coherence transfer through cross polarization, heteronuclear decoupling, and quadrupolar nuclei.

All the examples may be run through the web platform EasyNMR here: <https://easynmr.pastis.dk/arns>. The SIMPSON input files are also available on nmr.au.dk for local execution of the program. All figures in this chapter displaying simulations as a result of the example files provided with this chapter are plotted using EasyNMR.

3.1 CSA static and MAS

The first example covers the orientation-dependence of tensorial nuclear spin interactions as well as the concept of powder averaging. At the end, simulations of the same spin system under MAS are introduced, and the resulting spectra compared with the static case.

We start by setting up the spin system for a single ^1H nucleus with an isotropic chemical shift of 0 ppm and a chemical shift anisotropy of 10 ppm for an axially symmetric shift tensor ($\eta = 0$). If we orient the spin parallel to the reference frame (corresponding to $\text{P} \rightarrow \text{C}$ Euler angles of $\Omega_{PC} = (0, 0, 0)$, the entire spin system is defined by:

```
spinsys {
  channels 1H
  nuclei 1H
  shift 1 0p 10p 0 0 0 0
}
```

Bear in mind that which the keyword `shift` is an instruction that takes seven numeric arguments: `<index>` `<iso>` `<aniso>` `<eta>` `<alpha>` `<beta>` `<gamma>` (Fig. 1).

We perform our simulation on a static sample in a virtual spectrometer operating at 400 MHz proton frequency. Our simulation includes 2048 points of the FID, and we keep a spectral width of 20,000 Hz. To simplify our simulation, we set our starting operator to I_x for spin number 1 (11x) and define the detect operator as $I_+ = I_x + iI_y$ for spin 1 (11p). Thereby, the entire parameter section is given by

```
par {
  spin_rate      0
  np             2048
  proton_frequency 400e6
  start_operator 11x
  detect_operator 11p
  method        direct
  crystal_file   alpha0beta0
  gamma_angles  1
  sw            20000
  variable tsw   1.0e6/sw
  verbose       1101
}
```

We further specify that crystallite averaging should use the crystal file `alpha0beta0`, which corresponds to a single crystallite with angles $(\alpha_{CL}, \beta_{CL}) = (0, 0)$ implying that the crystal frame is aligned with the laboratory frame. Hence, in this case the chemical shift tensor is aligned with the laboratory frame.

The pulse program is in this case just acquisition of our signal:

```
proc pulseq {} {
  global par
  acq_block {
    delay $par(tsw)
  }
}
```

After generating the FID, we add a 100 Hz apodization and zero-fill to 8192 points before the data is Fourier transformed and saved. This is controlled in the `main` procedure of the input file.

```

proc main {} {
  global par

  set f [fsimpson]
  faddlb $f 100 0
  fzerofill $f 8192
  fft $f
  fsave $f $par(name).csdf \
    -csdf -sfrq $par(proton_frequency) -name "Simulation"
}

```

We recommend the reader to read and understand the entire input file before performing the tasks in the following exercise. The exercise may be executed using the web platform EasyNMR here: <https://easynmr.pastis.dk/arns>.

1. Run the simulation and verify that the resonance lies at the expected position cf. Eq. (7). Try representing the x axis with either Hz or ppm on the axis.
2. Change the angle beta (in degrees) and see what happens to the spectrum. At least make sure to check the angles 0, 90, and 54.74 and compare with Eq. (7). Fig. 3A shows a number of simulations with different β -angles.
3. Change the crystal file from alpha0beta0 to an entry that allows to simulate a powder pattern. This may be done using the crystal file zcw28656, which is a powder with 28,656 crystallites distributed according to the algorithm of Zaremba, Conroy and Wolfsberg [26–28]. Using this crystal file, the spectrum becomes a powder pattern (see Fig. 3B).
4. If the crystallite has too few crystallites, e.g. by using the crystal file rep678, the spectrum will appear ragged indicating that there are not enough crystallites to provide a smooth converged powder lineshape. As a rough rule of thumb, several thousands of crystallites are required to provide a smooth lineshape simulation (see the grey spectrum in Fig. 3B).
5. Change the crystal file back to zcw28656 and change the asymmetry parameter. As evident from Fig. 3C, this moves the singularities in the spectrum as expected.

Turning to the MAS example, only few lines need be changed in the input file. In the parameter section, the `spin_rate` instruction should give the spin rate in Hz and the number of γ_{CR} -angles (specified by the instruction `gamma_angles`) should be larger than one (vide infra).

6. Use the MAS example file to and simulate the spectrum under 1 kHz MAS using 8 γ_{CR} -angles and observe the result. Spinning sidebands with

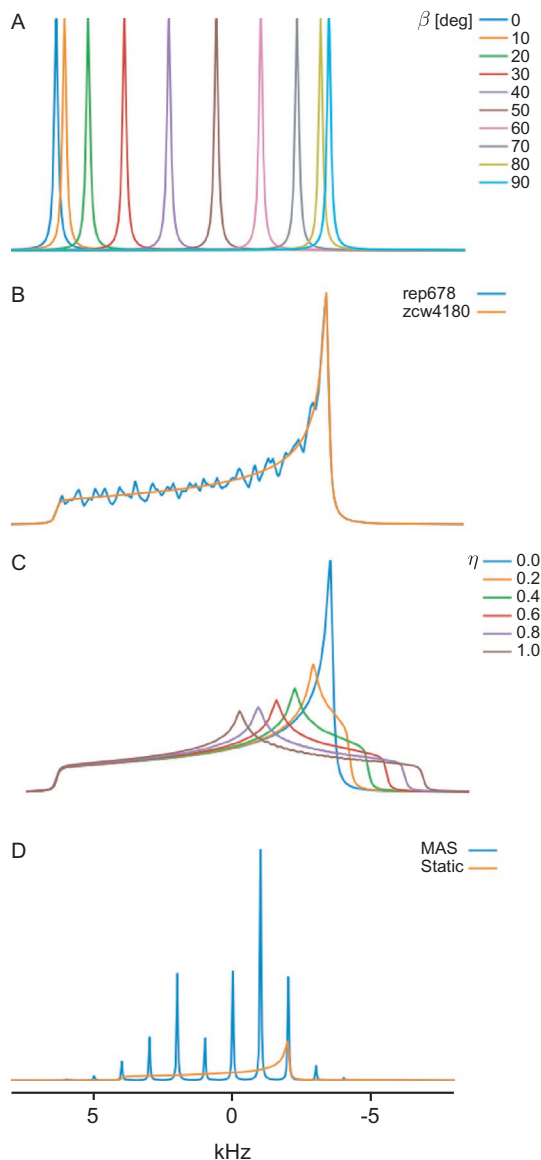


Fig. 3 Simulation of static spectra for a single ^1H atom with a chemical shift anisotropy of 10 ppm. (A) Spectra for different values for β_{CL} give resonances at different frequencies. (B) Overlay of simulations of a powder pattern with an insufficient number of crystallites (blue, rep678) or sufficient number of crystals (orange, zcw4180). (C) Simulations of powder patterns with different values for the asymmetry parameter (η). (D) Comparison between a static (orange) and a MAS (blue) simulated spectra.

negative intensity indicate that there is not sufficient of γ_{CR} -angles, so and you should increase the value for `gamma_angles` until a converged spinning sideband manifold is obtained. In this example, 16 γ_{CR} -angles should be enough.

7. Change the spin rate to different speed and use these simulations to observe how all spinning sidebands except the center band (located at the isotropic shift) move.

The simulation resulting from point 6 above is shown in Fig. 3D and is compared with the corresponding static simulation. As a rule of thumb, the number of γ_{CR} angles for a MAS simulation should be larger than the number of spinning sidebands observed in the spectrum. Simulation of a spinning sideband manifold requires substantially fewer crystallites than a static powder pattern, so a general advice is to choose a few hundreds of α_{CR} , β_{CR} -crystallites for a MAS spinning sideband manifold whereas a powder pattern requires thousands of crystallites.

3.2 ^1H decoupling

High-power decoupling in solids at low or moderate spinning speeds is a challenging task due to the strong dipolar interactions present in solids. Several pulse schemes have been proposed to ameliorate this task. Two-pulse phase modulation (TPPM) [33], XiX [34], and SPINAL-64 [35] are just a few commonly used sequences. SIMPSON is a perfect tool to examine the performance of such sequences. Here, we will investigate the TPPM and XiX pulse sequences, both of which can be represented by the pulse sequence shown in Fig. 4A, and which have also been mapped into the recent Unified Two-Pulse heteronuclear Decoupling (UTPD) scheme [36]. For TPPM the maximum intensity is found when the pulse length τ_p corresponds to approximately a π -pulse and the TPPM angle is around 10–15° as shown in Fig. 4B. XiX is a special case where $\phi = \pi/2$ and the pulse length is significantly longer. The characteristics of this pulse sequence have been investigated in detail in Ref. [37] and are reproduced in Fig. 4C. Here, pulse lengths of quarter-integer multiples of the rotor period lead to recoupling conditions and thereby poor decoupling, while the non-resonant conditions in general perform better than TPPM.

The spin system used in this example is larger than for the previous example: Here we use the spin system of a $-\text{CH}_2-$ group with a carbon-13 atom including all three interatomic dipolar couplings. For the specification of the Euler angles of the dipolar couplings, we have aligned one of the C–H bonds

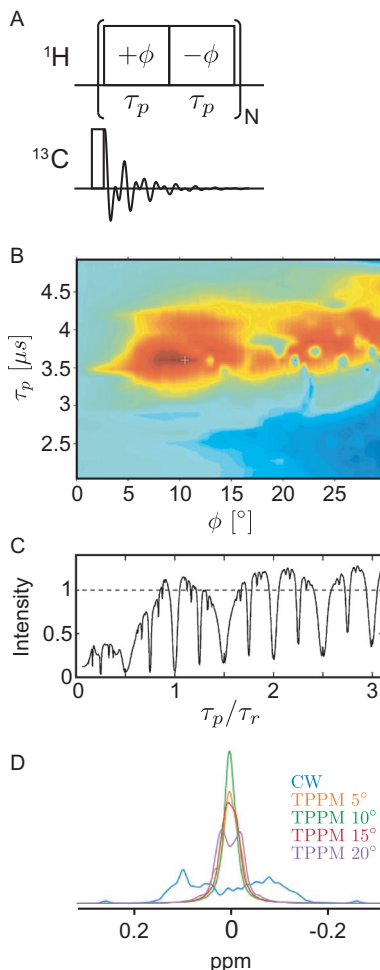


Fig. 4 (A) Pulse scheme for heteronuclear decoupling. (B) Experimental decoupling efficiency obtained using TPPM decoupling for Ca in glycine using a spin rate of 25 kHz and an rf field strength of 150 kHz for the decoupling. (C) Experimental decoupling efficiency of XiX for the Ca resonance of alanine using a spin rate of 30 kHz and an rf field strength of 150 kHz for the decoupling. The dashed line represents the intensity obtained with TPPM decoupling. (D) SIMPSON simulations of ^{13}C NMR spectra of a CH_2 group with CW or TPPM decoupling using different values for the TPPM angle. *Panel (B): Adapted from ref. I. Scholz, P. Hodgkinson, B.H. Meier, M. Ernst, Understanding two-pulse phase-modulated decoupling in solid-state NMR, J. Chem. Phys. 130 (2009) 114510 with the permission of AIP Publishing. Panel (C): Adapted from ref. A. Detken, E.H. Hardy, M. Ernst, B.H. Meier, Simple and efficient decoupling in magic-angle spinning solid-state NMR: the XiX scheme, Chem. Phys. Lett. 356 (2002) 298–304 with permission from Elsevier.*

(from C1 to H2) along the z axis of the crystal frame implying that the Euler angles of the dipolar coupling between nuclei 1 and 2 are all zero. The other C–H bond is inclined at an angle of 109.5° relative to the first C–H bond. The dipolar couplings strengths are 23.3 kHz and 21.3 kHz for C–H and H–H respectively. For the creation of bigger spin systems, go to the SIMMOL section for inspiration.

In the SIMPSON input file for TPPM we have chosen to control the angle ϕ by the Tcl variable `par(tppm_angle)` specified by the following line in the parameter section.

```
variable tppm_angle 15
```

and the acquisition using TPPM decoupling is achieved by the following pulse sequence.

```
proc pulseseq {} {
  global par
  acq_block {
    pulse $par(t180) $par(rf) $par(tppm_angle) 0 0
    pulse $par(t180) $par(rf) [expr -$par(tppm_angle)] 0 0
  }
}
```

where the decoupling is achieved using the two `pulse` instructions with the `rf` field strength `$par(rf)` on the hydrogen channel and zero on the carbon channel. Note that we have used the Tcl command `expr` to evaluate the expression providing the negative TPPM angle.

For XiX, we have chosen to specify the pulse length in fractions of the rotor period using the variable `par(xix_frac)` and the following acquisition statement in the pulse sequence.

```
acq_block {
  pulse [expr $par(tr)*$par(xix_frac)] $par(rf) x 0 0
  pulse [expr $par(tr)*$par(xix_frac)] $par(rf) -x 0 0
}
```

where the variable `par(tr)` is the rotor period. In both cases, the SIMPSON command `acq_block` seeks to find the most efficient way to propagate the evolution of the spin system by reusing propagators at different times if possible [23].

In the exercise, we compare the efficiency of `tppm` and `XiX` to that of continuous wave decoupling.

1. Run the three simulations and compare the results. Try varying the parameters defining the characteristics of TPPM and XiX (`tppm_angle` and `xix_frac`), and observe how they change the quality of the spectra.

2. Change the spinning speed to 111 kHz and evaluate the efficiency of decoupling in the low power condition (ca $\frac{1}{4}$ of the spinning frequency) [38]. You may have to increase the number of points to sample the entire FID.

The outcome of the simulations in point 1 is shown in Fig. 4D. These simulations demonstrate that both TPPM and XiX, when optimized, provide superior decoupling to conventional CW decoupling.

3.3 Cross-polarization

One of the most important application areas of the versatile numerical simulations offered by SIMPSON and other general-purpose NMR simulation programs is the examination and evaluation of pulse sequences. In other words, SIMPSON offers information about the stability of the pulse sequences towards variations in offsets, pulse strength and other parameters. To illustrate such an application, we will focus on heteronuclear coherence transfer using cross polarization [39]. This example investigates the cross-polarization pulse sequence for transfer of coherence from ^1H to ^{13}C for a simple two-spin model system. We will investigate the transfer as a function of the length of the mixing time and the rf field strengths on the two channels. We know that the Hartmann-Hahn match is obtained by the condition.

$$\nu_{\text{rf}}^I = \pm \nu_{\text{rf}}^S \pm n\nu_r, \quad n = 1, 2 \quad (8)$$

On the spectrometer, investigations of the transfer efficiency as a function of the mixing time would require acquisition of a number of experiments with different values for the mixing time, for which the total intensity would be examined as outlined in Fig. 5A. Since the total intensity in the spectrum is proportional to the first point in the FID, it is much more convenient just to sample the first point in the FID and then continue the propagation with the mixing pulse, since we do not have to worry about pulse deadtime etc. in numerical simulations. This scenario is outlined in Fig. 5B. It is once again the command `acq_block`, which is responsible for this stepwise incrementation of the mixing time. As we only sample the first point of the FID, the SIMPSON input file does not contain any command to Fourier transform the signal after end simulation.

As a final simplification of the simulation, we will assume that it is possible to perform an ideal 90° pulse, so we will not waste simulation time on calculating the effect of the first pulse on the ^1H channel. Instead, we will just set the start operator to $I_{2 \times}$ (I_x on channel 2, hydrogen) and detect the

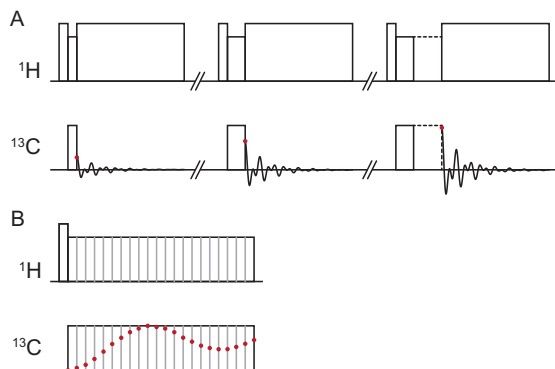


Fig. 5 Cross polarization pulse sequences. (A) Conventional setup for performing a series of experiments with increased contact time. The first point in the FID is indicated by a red dot. (B) SIMPSON simulation strategy for such an experiment, where only the first point in the FID is sampled for each contact time. Hence the simulation is performed as a one-dimensional simulation.

transferred coherence using I_{1x} (I_x on channel 1, carbon), so the pulse sequence reduces to

```
proc pulseseq {} {
  global par
  acq_block {
    pulse $par(tsw) $par(rfC) x $par(rfH) x
  }
}
```

To investigate the ability of the CP pulse sequence to transfer coherence between different spins, we first start by running a simulation of the transfer efficiency versus the mixing time using the above pulse sequence for a single ^{13}C - ^1H spin pair oriented along the magnetic field. The sample is static and we put 50 kHz RF field strength on both channels, and the mixing time is varied in steps of 5 μs (defined by the parameter $\text{\$par}(tsw)$). Since we sample 512 points ($\text{\$par}(np)$), the maximum mixing time is 2.56 ms.

Perform the following steps:

1. Run the simulation and observe the build-up for a single crystal of an isolated C-H spin pair.
2. Change the rf field strength on the ^{13}C channel. This is controlled by the line variable `rfC 50000` in the parameter section of the input file.

By changing this value, you move away from Hartmann-Hahn match leading to poorer transfer efficiency and a modulation of the periodicity of the transfer.

3. Change back `rfC` and modify the dipolar coupling. Look at the oscillation period of the build-up curve and see how this depends on the dipolar coupling strength.

Having established these basic tests, it is now time to investigate the spin dynamics of the CP pulse sequence for a powder sample. In a powder, the effective dipolar coupling will be modified by the factor $(3\cos^2\beta_{CL} - 1)/2$, according to Eq. (7), which will affect the oscillation frequency observed previously. CP simulations of static and MAS powder samples are investigated using the following steps:

4. Change the crystal file to `rep168` to make a powder simulation and observe the result.
5. Change to MAS by setting the spin rate and increasing the number of γ -angles to e.g., 8. Verify that the maximum intensity reaches the theoretical maximum of 73%, when appropriate values for the rf field strengths are used to fulfil the Hartmann-Hahn match for a spinning sample cf. Eq. (8). Try different conditions and observe the sign of the responding signal depending on the matching condition in Eq. (8).

3.4 REDOR

Sometimes, pulse sequences contain a number of repeated blocks, for which it will be convenient to reuse the propagators for these repeated blocks. The heteronuclear recoupling technique REDOR—rotational echo double resonance—introduced by Gullion and Schaefer [40] is a nice example of such a sequence. The pulse sequence is sketched in Fig. 6A. The pulse sequence typically starts with cross-polarization from hydrogen followed by an echo on the detected nucleus with repeated, rotor synchronized refocusing pulses on the third channel during the echo/mixing time. Two experiments are performed; the experiment with refocusing pulses on the third channel recouples the heteronuclear dipolar coupling (S), and a reference experiment without the refocusing pulses (S_0) to be able to compensate transverse relaxation during the experiment. A plot of S/S_0 as a function of the echo time allows determination of the heteronuclear dipolar coupling.

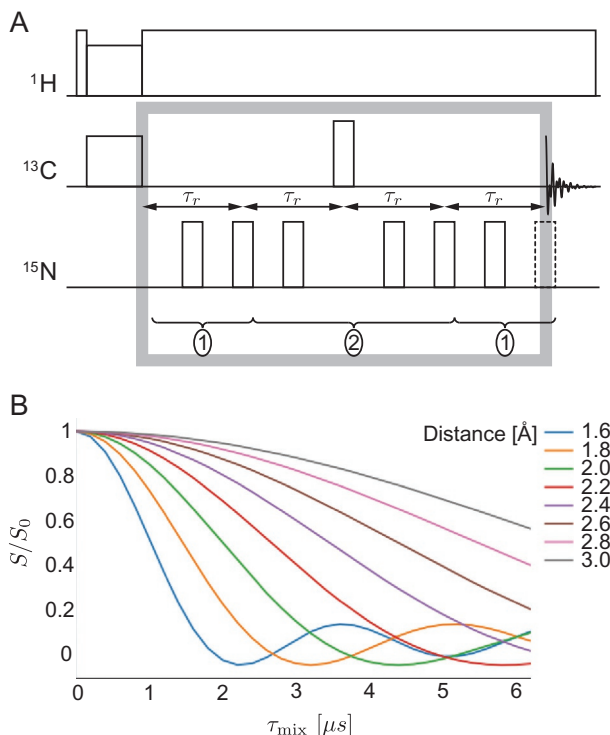


Fig. 6 (A) REDOR pulse sequence with indication of the part considered in the SIMPSON simulation framed in the grey box. Below the pulse sequence is indicated the propagators used in the efficient SIMPSON simulation (see text). (B) SIMPSON simulated REDOR dephasing curves for different distances for a ^{13}C - ^{15}N spin pair.

For the simulation of this pulse sequence, we will only consider the part framed by the grey box in Fig. 6A. For this reason, we omit the protons when defining the spin system and define only the ^{13}C and ^{15}N channels, the two spins and their dipole-dipole coupling.

```
spinsys {
  channels 13C 15N
  nuclei 13C 15N
  dipole 1 2 895 10 20 30
}
```

We perform the experiment at a 400 MHz spectrometer using a spin rate of 10 kHz. The density operator after the initial CP is given by $\mathbb{1}_x$, and we detect $\mathbb{1}_p$. We use the `par` section of the input file to define the rf field strength in Hz and calculate the rotor period (in μs) and pulse lengths.

We set the pulse power 50 kHz implying that the π -pulses will have a duration of 10 μ s. In REDOR, the increment of the mixing time corresponds to two rotor periods. In SIMPSON, we need to specify the spectral width for the dimension, which hence corresponds to $\nu_r/2$. The complete parameter section then reads.

```

par {
  np          32
  spin_rate   10000
  proton_frequency 400e6
  start_operator  I1x
  detect_operator I1p
  method      direct
  crystal_file rep66
  gamma_angles 8
  sw          spin_rate/2
  variable tsw 1e6/sw
  verbose     1101
  variable tr  1e6/spin_rate
  variable tr2 0.5e6/spin_rate
  variable rf  50000
  variable t180 0.5e6/rf
}

```

For simplicity and since REDOR is in general not too sensitive to rf imperfections, we will use the ideal pulse implementation available in SIMPSON [16] for all pulses. Ideal pulses are called by the command.

```
pulseid <duration> <rf> <phase> ...
```

identically to regular pulses. The difference is that although a pulse duration is specified, this value is only used to calculate the flip angle of the pulse. The ideal pulse has zero effective duration, making it easy to implement a rotor-synchronized pulse sequence.

The pulse sequence is more complicated than those in the prior examples and uses all the common pulse-sequence elements: pulses, delays, and acquisition instructions. The pulse sequence is implemented as a one-dimensional experiment following the same strategy as in the CP example above, such that only the intensity for each mixing time is sampled. Incrementation of the mixing period is controlled by the for loops that ensure that more and more pulses are employed on the ^{15}N channel:

```

proc pulseseq {} {
  global par

  acq
  for {set i 0} {$i < $par(np)-1} {incr i} {
    reset
    # First half of the sequence of  $\pi$ -pulses on 15N
    for {set j 1} {$j <= $i} {incr j} {
      delay $par(tr2)
      pulseid $par(t180) 0 0 $par(rf) x
      delay $par(tr2)
      pulseid $par(t180) 0 0 $par(rf) y
    }
    # Central echo with  $\pi$ -pulse on 13C
    delay $par(tr2)
    pulseid $par(t180) 0 0 $par(rf) x
    delay $par(tr2)
    # Second half of the sequence of  $\pi$ -pulses on 15N
    pulseid $par(t180) $par(rf) x 0 0
    for {set j 0} {$j <= $i} {incr j} {
      delay $par(tr2)
      pulseid $par(t180) 0 0 $par(rf) x
      delay $par(tr2)
      pulseid $par(t180) 0 0 $par(rf) y
    }
  }
  acq
}
}

```

Note that we need not record the S_0 reference spectrum, as there is no relaxation in the SIMPSON implementation of REDOR. The brute-force simulation described above is time consuming, as the same pulse sequence elements are calculated over and over again. SIMPSON has a convenient solution to this problem; it is possible to calculate a pulse sequence block once, store its propagator, and reuse it again at a later stage. This is possible, whenever the (potentially time dependent) Hamiltonian providing the propagator is identical at several places in the pulse sequence. This also implies that when reusing propagators in a MAS simulation, the propagator can only be used at the same time relative to the rotor period to ensure fulfilment of this criterion.

The numbered brackets below the pulse sequence in Fig. 6A show the two different pulse sequence blocks that are repeated over and over again in

the REDOR pulse sequence. Hence, we calculate these two propagators for efficient simulation of the pulse sequence. The propagators are first calculated once and stored using the command `store <n>` and are reused through the `prop <n>`, leading to the simpler and faster REDOR implementation.

```

proc pulseseq {} {
  global par

  # Calculation of the first propagator
  reset
  delay $par(tr2)
  pulseid $par(tl180) 0 0 $par(rf) x
  delay $par(tr2)
  pulseid $par(tl180) 0 0 $par(rf) y
  store 1

  # Calculation of the second propagator
  reset
  # Acquisition of the first datapoint
  acq
  delay $par(tr2)
  pulseid $par(tl180) 0 x $par(rf) x
  delay $par(tr2)
  pulseid $par(tl180) $par(rf) x 0 x
  prop 1
  store 2
  # Acquisition of the second datapoint
  acq

  # Acquisition of remaining datapoint
  for {set i 2} {$i < $par(np)} {incr i} {
    reset
    prop 1
    prop 2
    prop 1
    store 2
    acq
  }
}

```

Clearly, this is a very compact but rather obscure way to implement the REDOR pulse sequence. However, this implementation is significantly

more efficient and leads to significant shorter calculation times. The provided input file allows to perform the simulation in a brute-force manner without reusing propagators or using an input file with propagators.

1. Try both input files to appreciate the improved speed of the propagator-programmed input file. These simulations show the dephasing as a function of the REDOR time. Vary the dipole coupling strength and examine the dephasing curve.

Fig. 6B shows some simulations representing different dipolar couplings, and the well-known dephasing curves are observed. This example may serve as an example for simulation of REDOR dephasing curves to compare with experimental curves. Importing experimental data into SIMPSON for a real fitting is a different challenge that we will address for a different type of experiments below.

3.5 Fitting an experimental spectrum

When fitting an experimental spectrum, we use an external Tcl optimization library that calls the SIMPLEX [41] algorithm. The algorithm varies a defined set of parameters to minimize a predefined function [42]. In this exercise, we wish to minimize the root-mean square (RMS) deviation between the experimental and simulated spectrum by changing the parameters for the chemical shift tensor governing the spinning-sideband manifold of the spectrum. Before doing that, it is convenient to condition the experimental spectrum by (i) ensuring that the baseline is correct, (ii) extracting the relevant region of the spectrum, and (iii) adjust the number of points in the experimental spectrum by interpolation to a Fourier number (2^n). If the experiment is performed using MAS, the range should preferably be an integer multiple of the spin rate to ensure the fastest possible simulations. We note that steps (ii) and (iii) are handled internally in some simulation packages like dmFIT [18] and STARS [15], but in SIMPSON we need to specify these things by hand. In the simulation example, these steps are done using the input file `baseline.in`, which performs no simulations but sets up the baseline ranges and defines the new spectral window for the experimental spectrum. The script uses SIMPSON's ability to load a spectrum (through the command `fload`) and process spectral data to perform the desired operations. For convenience, it returns three spectra: (1) the baseline corrected spectrum extraction, (2) the baseline, and (3) the baseline ranges. Plotting all three spectra gives a good impression of the quality of the baseline algorithm.

The experimental spectrum used here is a ^{13}C spectrum of hexamethylbenzene (HMB) recorded at 400 MHz using ^1H decoupling and a spin rate

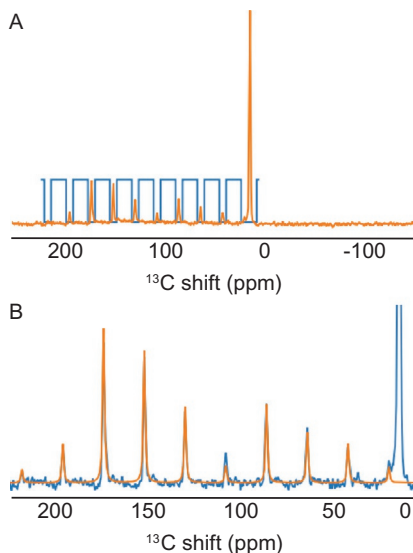


Fig. 7 (A) Experimental spectrum (orange) and base line regions (blue) for a 400MHz ^{13}C solid-state NMR spectrum of hexamethylbenzene. (B) Baseline-corrected expansion of the experimental spectrum (blue) and fitted CSA spinning-sidebands for the aromatic site.

of $\nu_r = 2200$ Hz. In the top of the script `baseline.in`, baseline regions are specified as intervals between the spinning side bands and the new spectral width that should be fitted. As shown in Fig. 7A, the spectrum shows a spinning sideband manifold in the range from 20 to 215 ppm and an intense peak at 14.5 ppm. The intense peak is attributed to the methyl groups, while the spinning sideband manifold is due to the CSA of the aromatic carbons. Upon executing the script `baseline.in`, we obtain a spectrum with reduced spectral width and information about the selected baseline. Fig. 7A also shows the selected baseline ranges.

To fit the CSA pattern, we pass the processed experimental spectrum into the SIMPSON input file `fit.in`, which loads the experimental spectrum using the instruction.

```
fload "baseline_0.spe"
```

in the main section of the input file. The fitting is performed using the Opt library [42] that is loaded using the instruction.

```
package require opt 1.0
```

in the top of the input file. The `opt` package is initialized, and the relevant fitting parameters are defined with the code.

```
opt::function rms
opt::newpar csa 100 2
opt::newpar eta 0.2 0.05
opt::newpar iso 130 0.1
opt::newpar lb 100 10 10200
```

The first line specifies that the library should minimize the return value of the Tcl function `rms`, which is specified in the input file. The remaining lines specify the parameters to optimize, their starting value, and the initial step size to establish the SIMPLEX kernel. The latter line has two extra (optional) numbers specified: The minimum and maximum values the parameter is allowed to take, in this case ensuring that the applied line broadening is between 10 Hz and 200 Hz. If no boundaries are specified, the algorithm allows an unconstrained optimization.

Fig. 7B shows an overlay of the processed experimental spectrum and the simulation to allow direct comparison. We observe an excellent agreement for the spinning sideband manifold of the aromatic site, suggesting that we found the correct parameters. Run the scripts `baseline.in` and `fit.in` in this order and observe the output.

A potential next step in an optimization is to assess the accuracy of the different parameters. To determine this, we typically calculate 95% confidence intervals for the individual parameters. With the `opt` package, this is a straightforward process that has previously been illustrated for different cases [23]. In addition, a thorough explanation of how the `opt` library calculates 95% confidence intervals is given in the accompanying documentation [42]. Fig. 8 reproduces such 95% confidence interval calculations for an optimization of the experimental ^{15}N spectrum of a peptide with a single ^{15}N labelled amino acid in oriented lipid bilayers. The spectrum is recorded using homonuclear decoupling and yields a doublet due to the ^1H - ^{15}N dipolar coupling. The asymmetry of the doublet may be explained by the presence of mosaic spread in the sample. The SIMPSON simulation convincingly reproduces the asymmetry as seen in Fig. 8A. The accuracy of the fitting parameters is assessed from the 95% confidence intervals shown in Fig. 8B showing the expected parabolic variation of the optimum rms deviation when a parameter is systematically varied.

3.6 Satellite transitions for quadrupolar nuclei

Quadrupolar nuclei represent a very exciting target for SIMPSON and other full density-matrix simulation programs, as such programs offer the possibility to exploit the combined effect of rf pulses and the quadrupolar coupling,

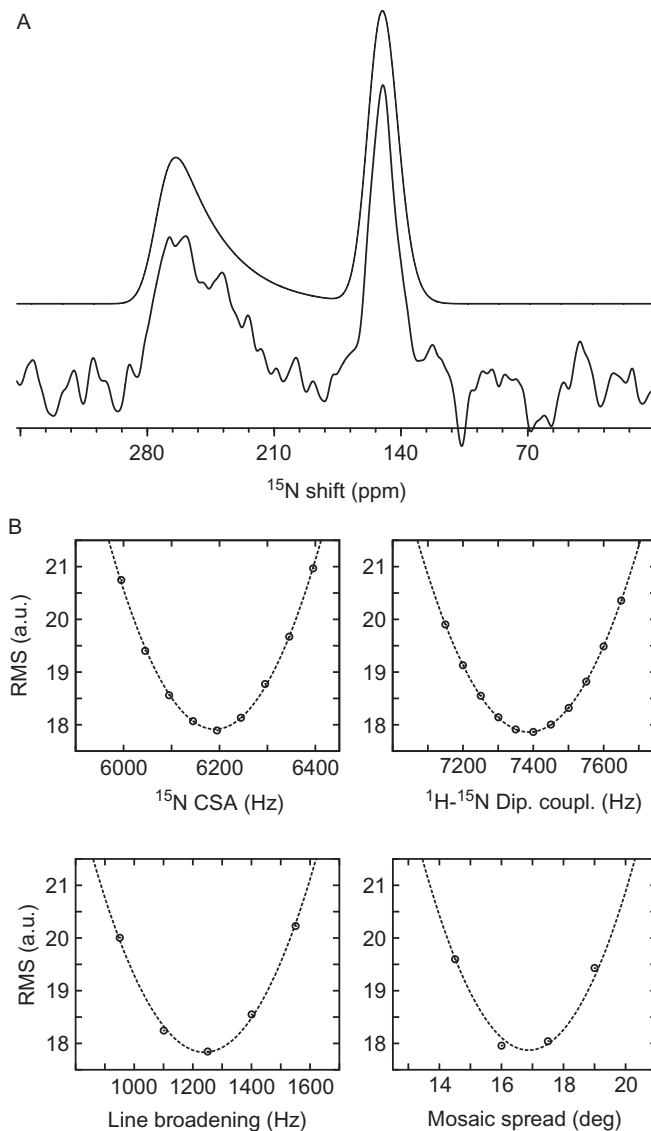


Fig. 8 Illustration of calculating 95% confidence intervals to determine the precision of fitted parameters. (A) Experimental (bottom) and simulated (top) ^{15}N spectra of alamethicin- ^{15}N -Aib8 in oriented lipid bilayers. The spectrum is recorded using ^1H FSLG decoupling resulting in an asymmetric doublet due to the ^1H - ^{15}N dipolar coupling in the amide and mosaic spread in the alignment [83]. (B) Calculations of 95% confidence intervals for the four parameters optimized. The solid lines represent the parabolic fit to the points. *Reproduced from Ref. Z. Tošner, R. Andersen, B. Stevansson, M. Edén, N.C. Nielsen, T. Vosegaard, Computer-intensive simulation of solid-state NMR experiments using SIMPSON, J. Magn. Reson. 246 (2014) 79–93 with permission from Elsevier.*

which is often too strong to neglect during the rf pulses. Such effects will be discussed further in the section on excitation of multiple-quantum coherences below.

Here, we will investigate the basic features of quadrupolar nuclei displaying satellite transitions depending on the nuclear spin and therefore we have omitted any pulses from the input file. First, we will investigate the position and intensities of the transitions observed for a single crystallite of a ^{27}Al (spin $I=5/2$). The quadrupole coupling tensor is setup by this line in the spin system description.

```
quadrupole 1 1 0.6e6 0.2 0 0 0
```

The first number represents the nucleus, the second indicates to which order in the Magnus expansion the quadrupole coupling should be considered. In this case the specification is that only the first-order quadrupolar interaction should be considered. The following two numbers are the quadrupolar coupling, C_Q , and the asymmetry parameter, η_Q , and the last three are the three Euler angles, Ω_{PC} , for the quadrupole coupling tensor. Since the first-order quadrupolar Hamiltonian is independent of the magnetic field strength, the proton Larmor frequency needs not be specified. The following steps give an illustrative introduction to quadrupolar nuclei, and selected simulations are shown in Fig. 9 for illustration:

1. Run the simulation of a single ^{27}Al nucleus and ensure you see the expected 5 lines corresponding to two outer satellites, two inner satellites, and a central transition.
2. Measure the intensity ratio between the lines. Ideally the ratio should follow the equation $I(I+1) - m(m-1)$.
3. Try the same simulation with ^{93}Nb (spin $I=9/2$) instead of ^{27}Al .
4. Change back the nucleus to ^{27}Al and the crystal file to `rep678` or even higher to get a nice powder pattern. Are the singularities located where you expected them to be? Bear in mind that pattern for each of the satellite transitions is just the powder pattern of a second-rank tensor, just like a CSA pattern.
5. When simulating a powder pattern of the satellite transitions, it may be convenient to use `I1p-I1c` as detect operator to remove the sharp central peak. The operator `I1c` represents the operator I_+ for the central transition of nucleus number 1.
6. Try similar simulations with different values for the asymmetry parameter. You may need to increase the number of crystallites for convergence of the line shape.

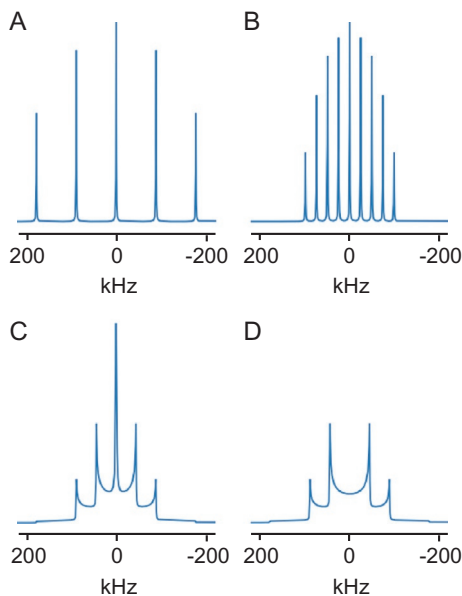


Fig. 9 Satellite transitions in quadrupolar nuclei. (A) Simulation of the NMR spectrum for a ^{27}Al nucleus in a single crystal with a quadrupole coupling of 600 kHz. (B) Same simulation, but for a ^{93}Nb spin. (C, D) ^{27}Al powder patterns for the same spin system as applied in (A). In (C) the detect operator is I_+ for all transitions, while the central transition is omitted in (D).

3.7 Second-order quadrupolar line shapes

When the quadrupole coupling becomes larger (some MHz) we will start to observe the second-order quadrupolar broadening of the central transition for quadrupolar nuclei with half-integer nuclear spin. Notably, this line broadening cannot be completely removed by MAS, only reduced. To investigate this effect, an example is provided for an ^{87}Rb nucleus with quadrupole coupling parameters of $C_Q = 3.3$ MHz, $\eta_Q = 0.2$ corresponding to the quadrupole coupling parameters of ^{87}Rb in RbClO_4 [43]. In order to compare the static and MAS spectra easily, the input file is constructed to simulate both at the same time. To do so, the static spectrum is simulated first, and then the spin rate and gamma angles are changed in the main section of the SIMPSON input in order to fit a MAS spectrum.

1. Run the simulation and observe the result. Are the singularities located at correct frequencies for both the static and MAS spectra? See for example recent reviews of Bain and co-workers [44,45].

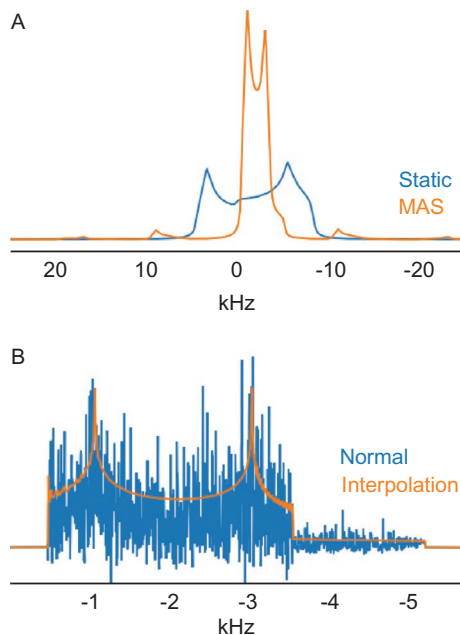


Fig. 10 (A) Simulated spectra showing the line shapes of the second-order quadrupolar interaction in ^{87}Rb static and MAS experiments for a nucleus with quadrupole coupling parameters of $C_Q = 3.3$ MHz and $\eta = 0.2$. (B) The MAS spectrum simulated using the normal time-domain simulation (blue) or using frequency-domain interpolation (orange), in both cases without applying any linebroadening.

2. What is—approximately—the center of gravity for the line? How does that match with the isotropic chemical shift of 0 ppm?
3. Try the two simulations with different values for the asymmetry parameter.

Fig. 10A shows the static and MAS spectra obtained by the input file of this example. The narrowing through MAS is clearly observed, but most notably we also observe that there is a significant second-order line broadening for both the MAS and static spectra.

A convenient feature of SIMPSON is the ability to use crystallite interpolation as explained elsewhere [23]. This is particularly interesting when simulating line shapes, where conventional powder averaging requires too many crystallites. To simulate the MAS spectrum above using crystallite interpolation, we specify the `methods` entry in the `par` section as well as the `crystal_file`, which now needs two sets of crystallites.

```
method          gcompute freq FWTASGinterpolation
crystal_file    LEBh/LEBh295 ROSELEBh/ROSELEBh4057
```


The method statement instructs SIMPSON to use the γ -COMPUTE algorithm [23], along with Fast Wigner Transform (FWT) [46] and Alderman-Solum-Grant [47] crystallite interpolation.

The efficiency of using crystallite interpolation is illustrated in Fig. 10B, where a simulation using the LEBh/ROSELEBh crystallites with 4057 crystallites is compared with the conventional simulation using a zcw crystal file with 4180 crystallites. It should be noted that the spectra are represented without any apodization.

3.8 RF pulses for quadrupolar nuclei

With large quadrupole couplings, we cannot neglect the quadrupolar interaction during RF pulses. This has implications for the choice of RF field strengths and pulse lengths. In the case of very strong pulses, we can neglect the quadrupole coupling interaction as we typically do with other interactions. This is typically referred to as the *strong-pulse* regime.

For half-integer quadrupolar nuclei, there exists an interesting *weak-pulse* regime, in which the pulse only affects the central transition while it leaves the satellite transitions untouched. Between the weak- and strong-pulse regimes, the effect of the rf pulse does not follow simple rules like the well-known fact that the flip angle in the strong-pulse regime equals the product of the rf field strength and the pulse length: $\theta = \tau_p \nu_{rf}$. In the weak-pulse regime, interestingly, the nutation frequency is different, because of the truncated Hamiltonian: $\theta = (I + 1/2)\tau_p \nu_{rf}$. Hence, the nutation frequency is doubled for a spin-3/2 nucleus when using a central-transition selective pulse (weak-pulse regime). Fig. 11 illustrates this effect through

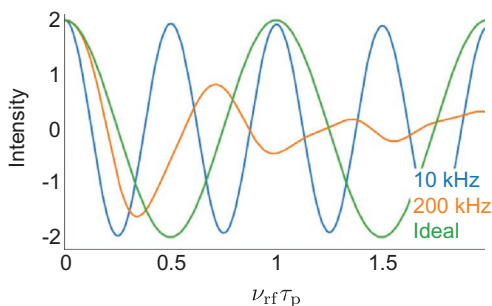


Fig. 11 Nutation curves showing the intensity as a function of the pulse length for a ^{87}Rb atom experiencing a quadrupole coupling of 1 MHz. The nutation curves represent rf field strengths of 10 kHz (blue) and 200 kHz (orange) as well as for an ideal pulse.

plots of the intensity as a function of the product of the pulse length and rf field strength for a ^{87}Rb nucleus (spin- $3/2$) experiencing a quadrupole coupling of 1 MHz. This figure clearly illustrates the conventional (corresponding to the strong-pulse regime) and the central-transition selective regimes as well as the nutation curve for an intermediate rf field strength providing a distorted nutation curve.

The exercise investigates this effect in detail by addressing the following points.

1. Run the simulation and check the nutation frequency. We expect to be in the central-transition selective regime for the present setup.
2. Try to vary the RF field strength and see if there are any values for which you obtain the expected nutation frequency. (Hint: try going to lower RF field strengths).
3. Change the spin system to perform the simulation for a ^{27}Al nucleus ($I = 5/2$). What happens to the nutation frequency?

3.9 Triple-quantum coherence excitation in MQMAS experiments

The MQMAS experiment [48] providing high-resolution NMR spectra of half-integer quadrupolar nuclei with large quadrupole couplings has significantly impacted the field of quadrupolar nuclei. The experiment is simple to setup and is very stable. However, relying on excitation and reconversion of the “forbidden” triple-quantum (3Q) transition, the experiment is associated with low sensitivity. Hence, it is important to find the optimum parameters for the excitation and mixing pulses. SIMPSON is an ideal tool to investigate this. The example provides simulations of the 3Q excitation and for the $3\text{Q} \rightarrow 1\text{Q}$ mixing as a function of the pulse length and for different mixing schemes.

To simulate the 3Q coherence buildup during a pulse we do not need to simulate a whole spectrum. We will just acquire the triple-quantum coherence using SIMPSON. In the pulseq procedure we specify the detection matrix by the command `matrix set detect coherence {3}`. The pulse sequence is otherwise quite similar to the CP simulation above, however only using a single channel. Execute the input file and verify the resulting fid.

1. At what pulse length is the maximum intensity?
2. Vary the quadrupole coupling constant in the range 2–10 MHz and note down the maximum excitation efficiency. What do you observe?

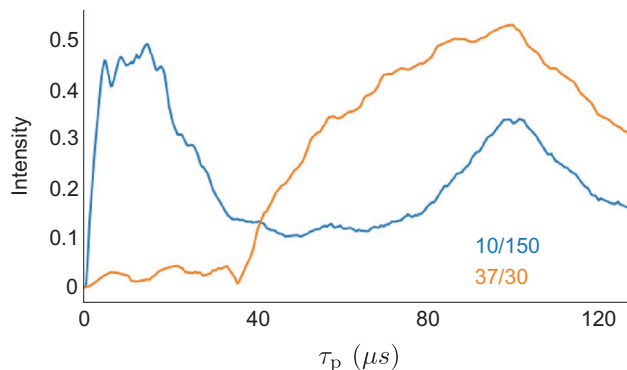


Fig. 12 Simulated excitation transfer efficiencies of 3Q coherences for ^{87}Rb with quadrupole coupling parameters of $C_Q=3.3$ MHz, $\eta=0.2$ using $\nu_R=10$ kHz/ $\nu_{\text{rf}}=150$ kHz (blue) and $\nu_R=30$ kHz/ $\nu_{\text{rf}}=37$ kHz (orange).

3. Use a quadrupole coupling constant of 3.3 MHz, and this time try to vary the rf field strength from 50 to 500 kHz. What do you observe?
4. Set the spinning frequency up to 30 kHz and the rf power down to 37 kHz and compare the simulation with the first 100 kHz simulation. Which one has the better sensitivity?

Fig. 12 shows two simulations of the 3Q coherence buildup as a function of the pulse length. The two examples vary by their spin rate and include a conventional “brute force” excitation using 200 kHz for a sample spinning at 10 kHz. The other example exploits the FASTER resonance condition [49] for a sample spinning at 30 kHz. The FASTER condition states that 3Q coherences are efficiently excited with low rf field strengths in between resonance conditions occurring at half-integer multiples of the rotor frequency. Indeed, a choice 37 kHz rf field strength (avoiding the resonance conditions at 30 kHz and 45 kHz) provides excellent 3Q excitation efficiency as evident from Fig. 12.



4. SIMMOL

While SIMPSON and other general-purpose simulation software programs allow simulation of essentially any spin system, it still remains a complex task to establish such spin systems with the correct orientation of all the tensorial spin interactions. For this purpose, we developed the SIMMOL program to help constructing such multispin systems for protein

molecules [50]. This program allows to load existing protein structures (or generate synthetic poly-alanine chains with specified torsion angles) and use the PDB structure to generate the spin system and provide 3D visualization of the molecular structure with user-defined representation of relevant atoms, bonds, peptide planes, coordinate systems, and anisotropic interaction tensors.

4.1 Establishment of a spin system

To illustrate how the generation of a larger spin system is performed with SIMMOL, we wish to setup a spin system aiming to visualize a large spin system of strongly coupled hydrogen atoms in a protein. The use of this spin system in an actual simulation will be addressed in a separate section on ultrafast MAS below. The model spin system will be selected from the SH3 protein, which is commonly used as a model protein system in solid-state NMR. Specifically, we wish to focus on the SH3 domain of the human RAS P21 protein activator, for which the protein structure is reported as PDB ID 2M51 and the chemical shifts are reported in the BioMagResBank under ID 19033. For this example, we focus on the amide hydrogen of Leu44 and assume that the network of hydrogens can be represented by all hydrogens within 4 Å of Leu44-HN. As outlined elsewhere [50,51], we assume that the CSA of the amide hydrogens can be represented by a tensor of a specific orientation relative to the peptide plane of the amino acid with a magnitude of $\delta_{\text{aniso}} = 7.7$ ppm and an asymmetry parameter of $\eta = 0.65$ [50]. For alpha protons, the corresponding values are assumed to be $\delta_{\text{aniso}} = 5.5$ ppm and $\eta = 0.12$. For all other hydrogens, we assume that there is no chemical shift anisotropy. For all hydrogens, we take the isotropic chemical shifts from the BMRB ID 19033.

The example is commented to explain the role of the individual elements. In brief, the molecule is loaded, and default values for the tensorial interactions are setup using the following commands

```
set m [mload 2M51.pdb]
mloadtensors $m -default
```

Next, Leu44-HN is selected and stored in the atom buffer 1

```
mselect $m 1 atom H residue &44
```

Following this, we select all other hydrogens and assign dipolar couplings for distances within 4 Å away from Leu44-HN by the commands

```
mselect $m 2 atom H*
set dipoles [mdipole $m 1 2 0AA 4AA]
```

where we have chosen to store the output of the `mdipole` command as the variable `dipoles`. The return value from this command is a Tcl list that for each dipole-coupled spin pair returns information about the dipolar coupling. In this example, the `$dipoles` contains.

```
{{461 720} -2405.10 {0 111.204 -115.572}} \
{{707 720} -13571.8 {0 98.1711 -176.192}} \
{{720 721} -5656.99 {0 80.8573 -131.456}} \
{{720 722} -5116.14 {0 128.384 -178.698}} \
{{720 723} -2690.14 {0 100.606 -168.168}} \
{{720 724} -20769.4 {0 87.2539 133.757}} \
{{720 742} -4524.57 {0 137.63 -77.2703}}
```

That is, a line for each dipolar spin pair consisting of a list with three elements: (i) a list containing the two atom numbers involved in the dipolar coupling, (ii) the coupling strength, and (iii) the Euler angles specifying the orientation of the dipolar coupling. In general, these return values are not needed, but in the present example, we wish to use them to establish the homonuclear ^1H - ^1H dipolar couplings in the spin system as well as the chemical shifts for each atom. Hence, we create a unique list of all the atoms by the following commands.

```
set atoms {}
foreach d $dipoles {
  set atoms [concat $atoms [lindex $d 0]]
}
set atoms [lsort -unique $atoms]
```

The first line creates an empty list named `atoms`. The `foreach` loop sequentially assigns the variable `d` to each of the elements in the list elements in `$dipoles` and appends the two atom numbers (first element of the line, obtained by the command `lindex $d 0`). Finally, as the atom number 720 occurs numerous places in the final list, multiple occurrences are removed by replacing the `atoms` list by its unique values, obtained by the last line. The variable `$atoms` now contains the following list

```
461 707 720 721 722 723 724742
```

which are the atom numbers (from the PDB) for the atoms involved in the spin system.

With this list of atoms, we may now assign the chemical shifts for which we have generated an array named `cs`,

```
set cs(LEU44,HB3) {1.343 0 0}
set cs(ARG45,H) {8.452 7.7 0.65}
set cs(LEU44,HG) {1.443 0 0}
set cs(LEU44,H) {8.841 7.7 0.65}
set cs(LEU44,HA) {4.049 5.5 0.12}
set cs(ASN43,HA) {4.409 5.5 0.12}
set cs(LEU44,HB2) {1.483 0 0}
set cs(PHE28,HA) {5.659 5.5 0.12}
```

Furthermore, we create a coordinate system aligned with the laboratory frame by the command

```
msetcoordsys $m {1 0 0} {0 0 0} {0 1 0}
```

since we need to specify a user-defined coordinate system for the tensorial interactions of all atoms not associated with a peptide plane. We then use the `foreach` command to loop over the atoms

```
foreach a $atoms {
  set at [mselect $m 1 atom $a]
  set type [lindex $at 0 1]
  set key "[lindex $at 0 3][lindex $at 0 2],$type"
  if {$type == "H"} {
    mshift $m 1 -magnitude $cs($key)
  } else {
    mshift $m 1 -magnitude $cs($key) -angles {0 0 0} -usecoordsys
  }
  mselect $m 2 atom |$a
}
```

The final line in the loop is just to append each atom to buffer 2, such that we can calculate all dipolar couplings between the atoms by

```
mdipole $m 2 2 0AA 0Hz
```

Remember that the last two arguments of the `mdipole` command are the bounds of the dipolar couplings, specified either by the distance in Ångström (using the unit `AA`) or by the value in Hertz.

The spin system generated through this example is shown in [Fig. 13](#) along with the graphics output showing the backbone cartoon rendering of all the

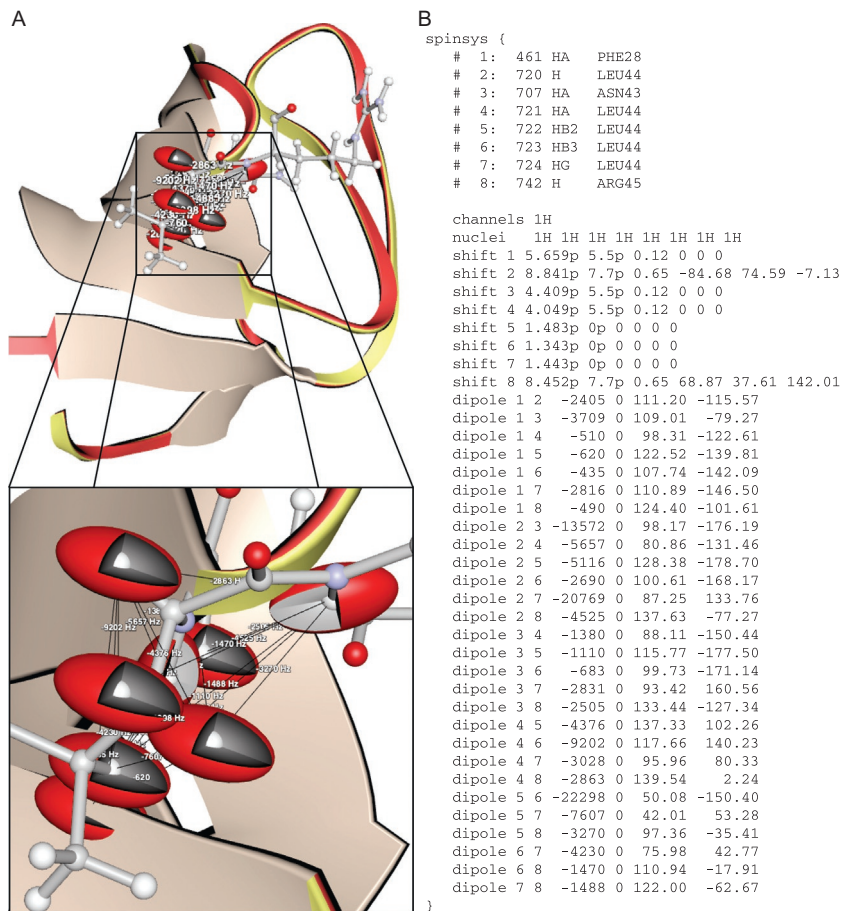


Fig. 13 (A) SIMMOL-generated representation of the SH3 protein highlighting the cartoon representation of the protein backbone and with a ball-and-stick representations of the atoms of residues 43–45. The figure also visualises the chemical shift tensors of selected atoms (see text) as red ellipsoids as well the homonuclear dipolar couplings between these hydrogens. (B) SIMPSON-formatted spin system output for the SH3 spin system generated using SIMMOL.

molecule. Furthermore, the graphical output highlights atoms and bonds of amino acids 43–45 and visualises the dipolar couplings and chemical shift tensors defined by SIMMOL. The spin system is given in SIMPSON format, so it is ready to include in a SIMPSON input file.



5. NMR simulations of proteins and peptides

5.1 PISA wheels

SIMMOL exists as a standalone program, but it also exists as a Tcl library that may be included into SIMPSON. In some cases, this is convenient, since it allows us to generate spin systems ‘on the fly’ from within SIMPSON, if specific spin systems are required. This feature is relevant, for example, if we wish to simulate a separated-local field (SLF) experiment like PISEMA [52] for a uniformly ^{15}N labelled α -helical protein. It is well-established that such SLF spectra will provide a set of resonances that form a characteristic wheel pattern depending on the membrane-bound conformation of the helix [53,54], termed PISA wheels. Such wheels have been simulated previously both by using SIMMOL and other software [51,55,56]. Here, we demonstrate how to perform such simulations using SIMPSON in combination with SIMMOL.

First, we load SIMMOL into SIMPSON through the command.

```
package require Simmol
```

This makes all the SIMMOL commands available in SIMPSON, so we can construct an α -helical protein (torsion angles -65° , -40°) through the command.

```
mmake 3 -65 -40
```

This peptide is then rotated by the `mrotate` command, and the ^{15}N chemical shift and ^1H - ^{15}N dipolar coupling for the backbone amide are calculated by the commands.

```
set shift_angles [lindex [mshift $m 1] 0 2]
set dipole_angles [lindex [mdipole $m 1 2 0AA 0Hz] 0 2]
```

where the returned Euler angles from commands `mshift` and `mdipole` are used as input for SIMPSON when doing the simulation by the command.

```
set g [fsimpson [list \
  [list shift_2_alpha [lindex $shift_angles 0]] \
  [list shift_2_beta [lindex $shift_angles 1]] \
  [list shift_2_gamma [lindex $shift_angles 2]] \
  [list dipole_1_2_beta [lindex $dipole_angles 1]] \
  [list dipole_1_2_gamma [lindex $dipole_angles 2]] \
]]
```

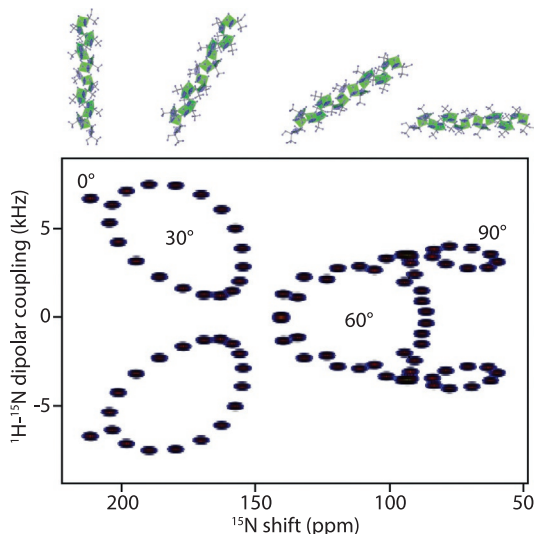



Fig. 14 Simulation of PISEMA spectra for α -helical peptides with different orientations relative to the magnetic field. (See text for details.) The peptide conformation is visualized above the spectrum and its tilt angle relative to the magnetic field indicated in the spectrum.

Having specified the Euler angles for the tensorial interactions ‘on the fly’ when starting the simulation, implementing a SLF pulse sequence like PISEMA is simple, based on our previous knowledge on implementing pulse sequences. Examples of PISEMA spectra resulting from this example for different helix conformations is shown in Fig. 14, where the wheel shapes (PISA wheels) are clearly visible.

5.2 Ultrafast magic-angle spinning

Current technology of magic angle spinning (MAS) allows to rotate the sample at frequencies reaching up to about 130 kHz [57]. To achieve higher rotation rates, smaller rotors are used. The loss of measurable material is compensated by increased sensitivity of smaller RF coils, narrower resonances, and by detection of more sensitive nuclei like protons. Besides improved resolution of ^1H spectra, faster MAS brings longer coherence lifetimes which allows application of sophisticated multidimensional experiments on biological/protein samples in a similar fashion to solution state studies [58].

However, it turns out to be extremely difficult to average homonuclear dipole-dipole interactions in densely coupled proton networks [59]. Using 100 kHz MAS spinning and 850 MHz ^1H Larmor frequency, linewidths on

the order of 300 Hz are reported for β -Asp-Ala dipeptide [60]. It is known that higher magnetic fields help to decouple inter-proton interactions due to larger separation of the partners in their chemical shifts [59]. Proton dilution by deuteration of protein samples is another popular route to increase the resolution [61]. Using a polycrystalline ubiquitin sample, amide proton line widths are reported to be about 100 Hz (126 kHz MAS frequency, 850 MHz) for fully protonated sample, and about 20 Hz for perdeuterated protein with all amide hydrogen atoms back-exchanged (120 kHz MAS frequency, 850 MHz) [57].

There is a hope that even faster spinning and even higher magnetic fields will remove the necessity of deuteration. But how fast should the rotation be? Two recent studies [57,62] predict that MAS frequencies on the order of 1 MHz are required to reach solution-like line widths. Such extrapolations are based both on experimental observations and mainly numerical simulations.

In this example, we will use SIMPSON to set up MAS rates and B_0 field conditions that are far from being realized in a real NMR spectrometer. We will focus on simulation of ^1H line shape for an amide proton of Val-44 residue of the SH3 domain. The spin system used here was established in the SIMMOL example above.

We will calculate the spectrum using the γ -COMPUTE algorithm in a frequency domain for the efficient simulation of the large spin system [23]. Using frequency domain calculation, we are free to choose the spectral width and number of points. Since we plan to increase MAS rate, we should consider proper setting of the time-step used for integration of the equation of motion by the SIMPSON parameter `maxdt`. It should be sufficiently short in order to follow changes in Hamiltonian even under ultrafast spinning. The γ -COMPUTE algorithm works in a way that it splits one rotor period in `par(gamma_angles)` steps and thereby decreases `maxdt` automatically when the spin rate is increased. We use these parameters.

```
par {
  spin_rate      110000
  proton_frequency 1e9
  method        gcompute freq block_diag dsyev
  np            16384
  start_operator Inx
  detect_operator I2p
  crystal_file   rep66
  gamma_angles   8
  sw            30000
}
```

where specifically the entry method needs attention. The specification above sets up a simulation using γ -COMPUTE in the frequency domain with block diagonalization of the matrices whenever possible, and uses the dsyev algorithm for diagonalisation of the Hamiltonian in order to evaluate its matrix exponent. For further details about the method, see Ref. [23]. The pulse sequence code uses the `acq_block` to acquire the spectrum.

```
proc pulseseq {} {
  global par

  acq_block {
    delay [expr 1.0e6/$par(spin_rate)/$par(gamma_angles)]
  }
}
```

The idea of the exercise is to run the simulation with different values for the spin rate to observe how large a spin rate is required before no further gain in resolution is obtained. Fig. 15 shows a series of spectra simulated with different spin rates. We see that the line shape consists of one sharp and one broad component that both are getting narrower as the MAS frequency increases towards extreme values. The broad component contains most of the signal intensity and is responsible for improvements in the peak amplitude. The sharp component, on the other hand, is responsible for experimentally observable peak width and resolution, since the broad component often contributes just to a baseline in a crowded 2D spectrum. The full-width-at-half-height does improve only slightly when increasing MAS frequency beyond 300 kHz. However, we obtain only about 25% of the available

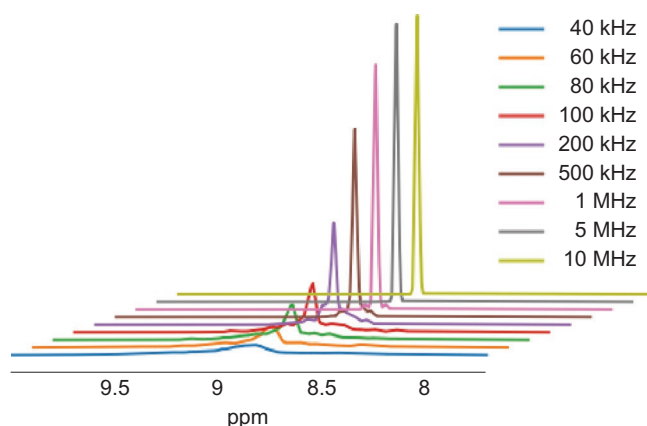


Fig. 15 Simulated ^1H spectra under ultrafast MAS employing spin rates indicated in the figure for an eight-spin system from the SH3 protein (see text for details).

signal amplitude. The peak height continues to increase dramatically with MAS frequency and settles only at about 5 MHz. Such spinning frequencies are clearly beyond all limits of a physical device.

5.3 NCOCA solid-state NMR optimization

With its versatility and function as a virtual spectrometer, we wish to optimize a ‘real’ experiment to tune the mixing times and transmitter carrier offset in an NCOCA correlation experiment that correlates backbone amide nitrogen with $C\alpha$ in the preceding residue through the carbonyl. We wish to use cross polarization for the heteronuclear transfer (termed double CP, DCP [63]) followed by POST-C7 [64] for the homonuclear transfer. Fig. 16A shows the schematic representation of the pulse sequence. For this example, we consider an 800 MHz spectrometer.

For each of the transfer steps, the transfer efficiency depends critically on the mixing/contact time and transmitter carrier offset. Since backbone amide nitrogens are typically not very dispersed with respect to their isotropic chemical shift, we assume that we can place the carrier on-resonance with the nitrogen. On the other hand, given that the backbone nitrogen is directly bonded to both the carbonyl on the preceding residue and $C\alpha$ on the same residue, we need to ensure that the transfer primarily goes to CO. This can be tuned by the carrier offset on the carbon channel since the carbonyl has a chemical shift of around 170 ppm, while $C\alpha$'s typically resonate around 50 ppm. Throughout the optimization, we will disregard the effect of hydrogens.

To investigate this transfer step, we use SIMMOL to generate a realistic spin system consisting of a backbone amide nitrogen and its directly bonded CO and $C\alpha$ atoms in a synthetic α -helix with torsion angles $\phi = -65^\circ$, $\psi = -40^\circ$ as seen in the online example. The resulting spin system is.

```
spinsys {
#      1      2      3
#      A2-N  A2-CA  A1-C
#
channels 15N 13C
nuclei 15N 13C 13C
shift 1 119p 99p 0.19 76.984 168.06 -17.701
shift 2 50p -20p 0.43 39.857 18.335 127.98
shift 3 170p -76p 0.9 -71.727 78.37 -4.4068
dipole 3 1 1304.7 0 71.671 -98.316
```

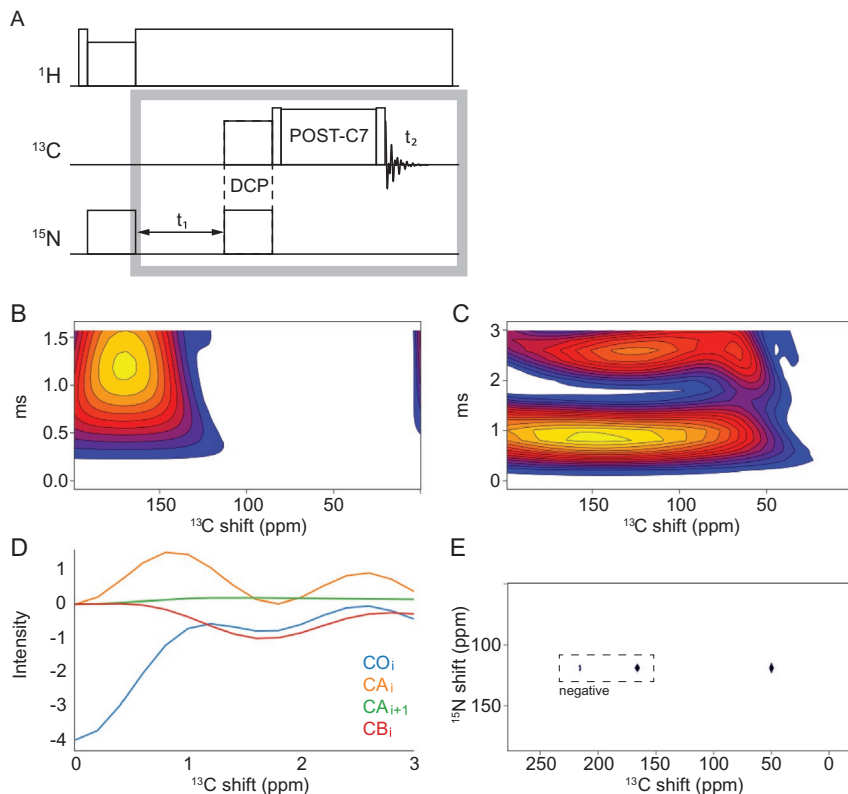


Fig. 16 Simulations of the optimizations necessary for an optimal NCOCA experiment using DCP and POST-C7. (A) Two-dimensional plot of the $\text{N} \rightarrow \text{CO}$ intensity as a function of the CP contact time and the transmitter carrier offset on carbon. (B) POST-C7 transfer intensity from $\text{CO} \rightarrow \text{CA}$ as a function of the mixing time and transmitter carrier offset. (C) Plot of the intensity of the CO , CA , and CB signals as a function of the POST-C7 mixing time. (D) 2D plot of the DCP-POST-C7 NCOCA experiment for a single site (see text for details).

```

dipole 3 2 -526.39 0 101.65 -91.974
dipole 1 2 988.16 0 128.61 -84.947
jcoupling 3 1 -15 0 0 0 0
jcoupling 1 2 -11 0 0 0 0
}

```

For each value for the carbon transmitter carrier offset, the DCP step is implemented as we did in the CP example above. To obtain a two-dimensional plot of the transfer intensity, we create an empty two dimensional spectrum using the `fcreate` command and move the one-dimensional

simulation of the transfer as a function of the contact time into the two-dimensional spectrum using the `findex` and `fsetindex` commands of SIMPSON. The resulting 2D plot is shown in Fig. 16B. It shows a clear maximum around 1.2 ms contact time and 34 kHz carbon (~ 170 ppm) carrier offset.

The second step is the homonuclear transfer from CO to C α , for which we will use the POST-C7 pulse sequence. The spin system for this transfer involves four carbons: CO, C α , and C β on the target residue and C α on the next residue. The latter is to ensure that the coherences do not leak to the neighbouring residues. The resulting spin system reads.

```
spinsys {
#      1      2      3      4
#      A1-C  A1-CA  A2-CA  A1-CB
#
channels 13C
nuclei 13C 13C 13C 13C
shift 1 170p -76p 0.9 -71.727 78.37 -103.63
shift 2 50p -20p 0.43 39.857 18.335 127.98
shift 3 50p -20p 0.43 39.857 18.335 127.98
shift 4 30p 10p 0 -98.452 122.65 84.753
dipole 2 1 -2142.4 0 133.91 177.8
dipole 2 3 -138.04 0 114.04 171.64
dipole 2 4 -2159.4 0 57.347 -95.247
dipole 1 3 -526.39 0 101.65 168.81
dipole 1 4 -489.19 0 41.169 -53.333
dipole 3 4 -86.178 0 57.826 -28.202
jcoupling 2 1 55 0 0 0 0
jcoupling 2 4 35 0 0 0 0
}
```

The POST-C7 pulse sequence element is designed for longitudinal homonuclear transfer, i.e. $\hat{I}_{1z} \rightarrow \hat{I}_{2z}$. As in the previous step, we will implement the two-dimensional optimizations as a series of one-dimensional simulations, each calculating the transfer as a function of the mixing time for a specific transmitter carrier offset. The resulting simulation is shown in Fig. 16C. The simulation shows that the best transfer is obtained at mixing time of 800 μ s and 30 kHz (~ 150 ppm) offset. The value for the transmitter carrier offset is in the expected range, since POST-C7 (and other pulse sequences for

homonuclear transfer) provide the best transfer if the carrier offset is centered between the two nuclei.

For experiments where a selective transfer is desired, it is interesting to use SIMPSON to follow the leakage of coherences to other nuclei. For this purpose, we employ the optimum transmitter carrier offset in a simulation, where we investigate the transfer from the carbonyl carbon to all the other carbon atoms in the spin system. The plot resulting from this simulation is shown in Fig. 16D and demonstrates the expected strong transfer to $C\alpha$ on the same residue, while only a little fraction is transferred to $C\alpha$ of the neighbouring residue. Interestingly, there is a relayed transfer to $C\beta$ at longer mixing times.

Finally, we wish to carry out a simulation of the entire pulse sequence for a single set of resonances by combining the optimized DCP transfer from ^{15}N to ^{13}C with the POST-C7 block for homonuclear transfer. The resulting spectrum is shown in Fig. 16E.



6. Optimal control

Optimal control theory has been developed to solve general optimization problems of steering dynamical systems in a desired way, to maximize outcome and/or to minimize the necessary resources [65–67]. In the context of designing NMR experiments, the Liouville–von Neumann equation provides a detailed description of dynamics for typical spin systems with specific internal spin interactions. Radiofrequency pulses are used as means of external manipulation to control the spin evolution. The quest is to find such pulse sequences that maximize transfers between known operators (or reproduce evolution under a particular effective Hamiltonian) [68,69]. Optimal control theory provides easy access to the first derivative of the objective function and allows to optimize tens of thousands of pulse parameters at once. It has been applied in NMR to improve sensitivity [70–72] or achieve specific features of the NMR experiment [73–75]. The success of the method originates from the ability to include a range of experimental limitations and hardware imperfections in the optimization process. This variability is demonstrated in the recent study of dipolar recoupling between ^{15}N and ^{13}C nuclei under MAS conditions where the sample rotation leads to temporal modulations of rf amplitudes and phases due to spatially inhomogeneous excitation field of solenoidal coils [71].

In this example, we focus on deuterium (^2H) and polarization transfer to ^{13}C in perdeuterated proteins. The challenge of experimental design comes from the fact that ^2H possesses a quadrupole moment that interferes strongly with the applied RF pulses. In the work of Wei et al. [76], optimal control was used to develop ^2H excitation pulse that corresponds to ideal 90° -pulse on spin-1/2 nuclei. Interestingly, the resulting optimal pulse sequence consists of isolated short pulses applied every rotor period. It is a nice example where numerical optimization leads to an analytical pulse sequence. Similarly, optimization of ^2H - ^{13}C polarization transfer became inspiration for development of RESPIRATION-CP method [77] which is applicable for spin-1/2 nuclei and which shows improved robustness towards rf inhomogeneity and rf amplitude mismatch.

Important parts of the SIMPSON input file for optimal control calculation [22] are the procedures `target_function` and `gradient`. The first function defines what quantity should be maximized, and the latter provides proper gradient of the target function. Through these procedures SIMPSON provides full flexibility in defining arbitrary target functions. In our case we optimize transfer starting from the ^2H operator $\rho(0) = I_{1x}$ and arriving to the desired ^{13}C operator $C = I_{2x}$, i.e. a transfer between two Hermitian operators. The pulse sequence is represented by two shaped pulses applied simultaneously to ^2H and ^{13}C rf channels. Each shaped pulse consists of `$par(NOC)` elements characterized by the amplitude and phase pairs. In the pulse sequence definition (procedure `pulseseq`) we use the command `oc_acq_hermit` instead of the usual acquisition in order to trigger calculation of a target function or the gradient. The procedure `target_function` takes a simple form of calling `fsimpson` calculating a single number according to the formula.

$$\Phi = \text{Tr} \{ C^+ U(0, T) \rho(0) U^+(0, T) \} \quad (9)$$

while the procedure `gradient` leads to calculation of a pseudo-fid containing first derivatives of the target function with respect to pulse element parameters. The length of this pseudo-fid corresponds to the number of elements in all optimized rf shapes, that is $2 * \text{par}(NOC)$ in our case. Optimization is invoked by the command `oc_optimize` in the main section and is controlled using several parameters. Besides the GRAPE algorithm with conjugated gradients (CG), SIMPSON also implements a quasi-Newton optimization using the limited memory Broyden-Fletcher-Goldfarb-Shanno algorithm (L-BFGS) [23]. The choice of algorithm is determined by setting `$par(oc_method)` variable to CG or L-BFGS. For L-BFGS, it is essential to use

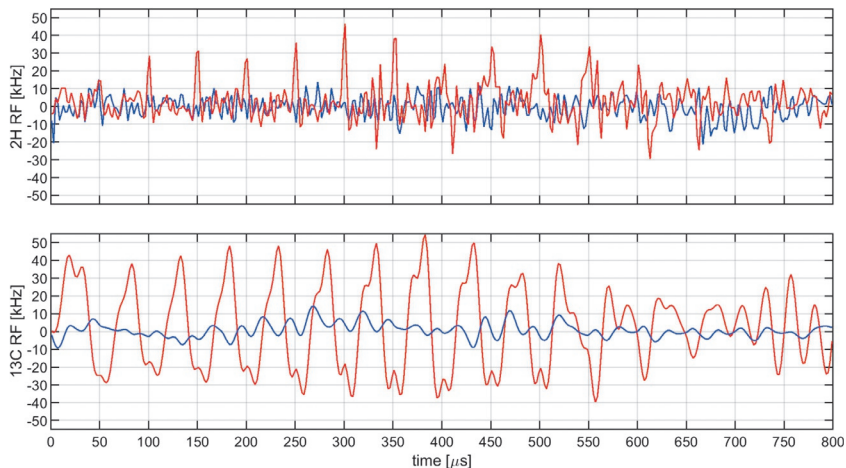


Fig. 17 Pulse shapes for ^2H (top) and ^{13}C (bottom) resulting from an optimal-control optimization of the $^2\text{H} \rightarrow ^{13}\text{C}$ coherence transfer in a directly bonded ^{13}C - ^2H spin system. The plots show the x and y components of the rf field strengths in red and blue, respectively.

higher precision gradients [78] which is controlled by parameter `$par (oc_grad_level)` set to the corresponding order of the gradient approximation.

The resulting RF shapes are presented in Fig. 17 as x- and y-components of the RF field. Note the short pulses spaced by $50 \mu\text{s}$ (corresponding to one rotor period at MAS frequency of 20 kHz) on the ^2H channel. On the ^{13}C channel we observe rf irradiation with alternating phase in a fashion similar to the RESPIRATION-CP.

In our example, all parameters are set such that SIMPSON calculation progresses reasonably fast. For a real application it is necessary to increase powder averaging, include rf field inhomogeneities and spread of chemical shifts or coupling constants. All of that averaging can easily be parallelized and done on a high-performance computing cluster [23]. An example implementation of chemical shift spread is included via procedures `get_lims` and `prepare_ave` that generate a text file with a list of parameter distributions. This file is then loaded automatically when the variable `$par (averaging_file)` is set to its name.

The optimization is prone to find local maxima and thus calculations should be repeated many times from different (random) initial guesses. But here we all start from the well tested initial shape of constant 1 kHz irradiation on both channels.



7. Dynamics

SIMPSON uses the Hilbert-space representation of the Hamiltonian, i.e. a representation where the Hamiltonian is represented as a matrix expanded by the wave functions of the Zeeman interaction. The advantage of using a Hilbert-space representation is the modest exponential growth of the matrix size with respect to the spin system size (see Eq. (4)) compared to the Liouville space, where the matrix is expanded by the spin operators \widehat{E} , \widehat{I}_x , \widehat{I}_y , and \widehat{I}_z . When dynamics and spin exchange is concerned, the Liouville-space representation has the advantage that it is always possible to relate a matrix element of the Hamiltonian to a specific spin operator, hence it is straightforward to simulate exchange by operations of the type $2\widehat{I}_{1z}\widehat{I}_{2x} \leftrightarrow 2\widehat{I}_{1x}\widehat{I}_{2z}$, while this is more complicated in Hilbert space.

In order to be able to simulate spin exchange, we proposed to use mixed Hilbert- and Liouville-space simulations in SIMPSON by using the versatile Tcl interface [79]. This allowed us to simulate ^1H -mediated spin exchange in the protein kaliotoxin [6] in a so-called CHHC experiment shown in Fig. 17A. The basic idea was to use SIMPSON to simulate the effect of the cross-polarization blocks using relatively small spin systems, while the spin exchange could then be simulated by considering exchange between spins. In fact, we did not use a full Liouville-space representation, as the pulse sequence uses longitudinal ($\widehat{I}_{1z} \leftrightarrow \widehat{I}_{2z}$) transfer, for which it is very efficient to use an exchange-matrix representation. The selection of spin systems and the resulting spectrum for kaliotoxin from Ref. [79] is shown in Fig. 18.

A simpler case is a two-site jump involving two spins with resonance frequencies of ν_A and ν_B , experiencing exchange with a rate constant k . In this case, the analytical expression for the spectrum is known.

$$s(\nu) = \frac{k(\nu_A - \nu_B)^2}{\pi^2(\nu - \nu_A)^2(\nu - \nu_B)^2 + k^2(\nu - \frac{\nu_A + \nu_B}{2})^2} \quad (10)$$

To implement this equation in SIMPSON, we can generate a spectrum by using the ability of SIMPSON to access the individual datapoints of the spectrum using the `findex` and `fsetindex` commands. The full sequence of commands could be implemented as a procedure.

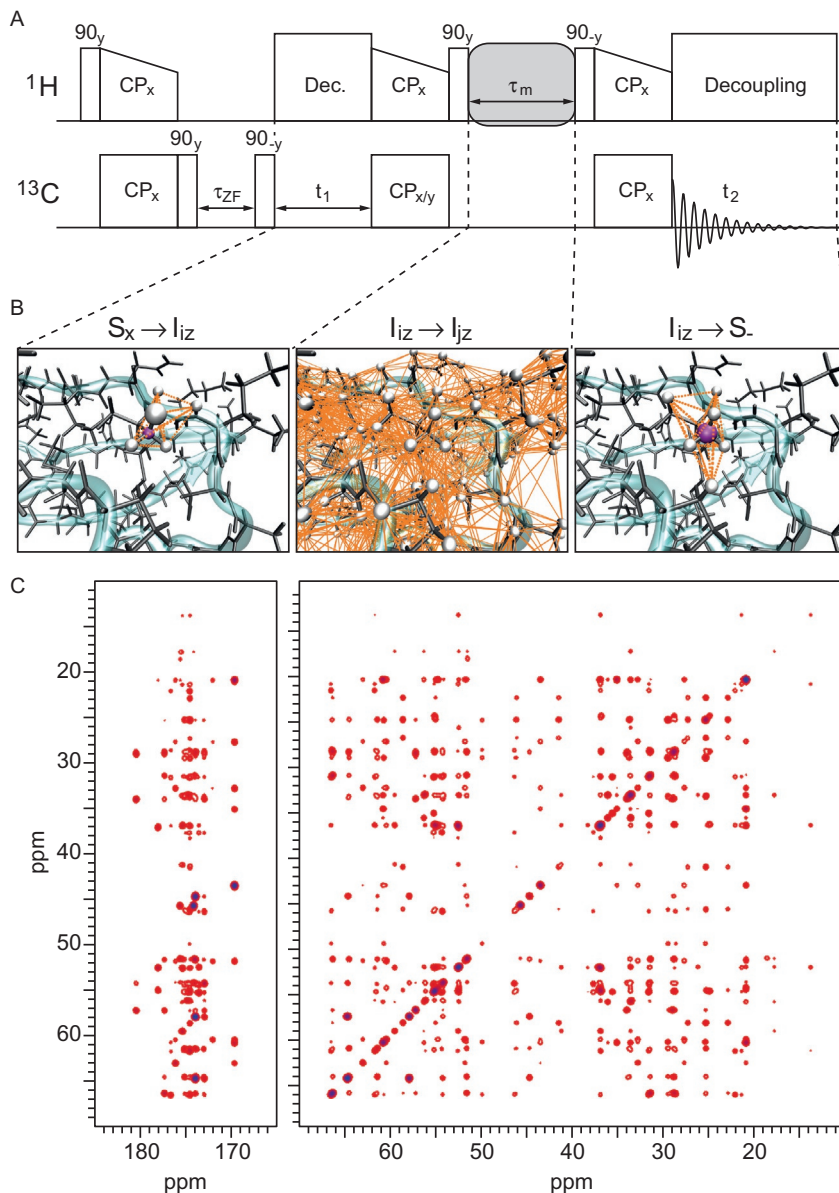


Fig. 18 SIMPSON simulations of spin exchange in a CHHC experiment. (A) The CHHC pulse sequence that uses cross-polarization blocks to transfer magnetisation from hydrogen to carbon and back, a mixing block in which spin exchange among the hydrogens occurs, and finally, a cross-polarization block to transfer magnetization to carbon for detection. (B) Illustration of typical selections of spin systems for the different blocks of the pulse sequence. (C) Simulated CHHC spectrum for the protein kaliotoxin. For further details see Ref. [79]. Adapted from Ref. T. Vosegaard, *Challenges in numerical simulations of solid-state NMR experiments: spin exchange pulse sequences*, *Solid State Nucl. Magn. Reson.* 38 (2010) 77–83 Copyright (2010) with permission from Elsevier.

```

proc fexchange {sw np nuA nuB k} {
  set f [fcreate -type spe -sw $sw -np $np]
  set dnu [expr ($nuA-$nuB)]
  for {set i 1} {$i <= $np} {incr i} {
    set nu [fx $f $i]
    set dnuA [expr $nu - $nuA]
    set dnuB [expr $nu - $nuB]
    set dnuAB [expr $nu - ($nuA+$nuB)/2.0]
    set s [expr $k*$dnu*$dnu/(9.8696044 \
      * $dnuA*$dnuA*$dnuB*$dnuB \
      + $k*$k*$dnuAB*$dnuAB)]
    fsetindex $f $i $s 0
  }
  return $f
}

```

In this implementation, we first create an empty spectrum using the `fcreate` command. The spectrum is then populated through the `for` loop over all points in the spectrum. For each point, we obtain the frequency by the command `fx`. The frequency is used to calculate the various frequency differences, which then are used in Eq. (10). Finally, the generated spectrum is returned by the procedure through the `return $f` instruction.

The two-site jump has the so-called coalescence point, where the intensity seems very low, since the lines are broad and partially overlapping. According to Bain [80], this occurs when $k_{\text{coalescence}} = 2\pi|\nu_A - \nu_B|/\sqrt{8}$. Fig. 19A investigates this effect through a spin system consisting of two nuclei with $\nu_A = -100$ Hz and $\nu_B = 100$ Hz with different values for the exchange constant. Indeed, we observe the characteristic coalescence lineshape in the middle spectrum ($k = 450 \text{ s}^{-1}$), which is very close to the expected coalescence point $k_{\text{coalescence}} \approx 444 \text{ s}^{-1}$. In this figure, we also observe the expected transition from two distinct peaks at slow exchange to one peak at fast exchange.

We can extend this approach to model two-site jumps to more advanced examples by merging it into SIMPSON. The goal is to simulate the ^2H solid-state NMR spectra of a phenylalanine amino acid undergoing ring-flip motion in a protein. The complication over the previous example is two-fold. First, the resonance frequencies of the deuterons are orientation dependent and need be calculated for each crystallite in the powder. Second, ^2H is a spin-1 nucleus, which has two single-quantum transitions.

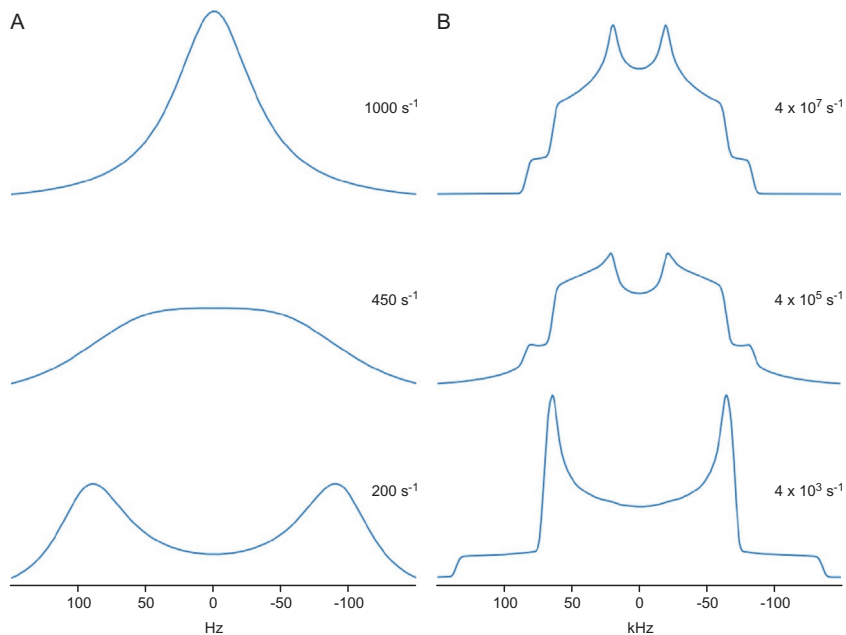


Fig. 19 SIMPSON simulations of chemical exchange. (A) Simple chemical exchange between two sites with resonance frequencies of ± 100 Hz and different exchange rates as specified in the figure. (B) Simulations of aromatic ring flip in phenylalanine measured by ^2H solid-state NMR with exchange rate constants specified in the figure.

The two-spin Hamiltonian for two ^2H nuclei will be of dimensions 9×9 and will have the diagonal elements $\langle m_1 m_2 | \hat{H} | m_1 m_2 \rangle$, where m_1 and m_2 represent the $m_z(+1, 0, -1)$ spin quantum number each of the nuclei. The single-quantum transition frequencies may be obtained as.

$$\begin{aligned}
 \omega_{1,+1 \leftrightarrow 0} &= \langle +1m | \hat{H} | +1m \rangle - \langle 0m | \hat{H} | 0m \rangle \\
 \omega_{1,0 \leftrightarrow -1} &= \langle 0m | \hat{H} | 0m \rangle - \langle -1m | \hat{H} | -1m \rangle \\
 \omega_{2,+1 \leftrightarrow 0} &= \langle m+1 | \hat{H} | m+1 \rangle - \langle m0 | \hat{H} | m0 \rangle \\
 \omega_{2,0 \leftrightarrow -1} &= \langle m0 | \hat{H} | m0 \rangle - \langle m-1 | \hat{H} | m-1 \rangle
 \end{aligned} \tag{11}$$

The idea is to calculate these frequencies and insert them into Eq. (9) for each of the transitions in SIMPSON by the Hamiltonian obtained by the command `matrix get hamiltonian`:

```

set h [matrix get hamiltonian]
set w11 [expr [lindex $h 0 0 0] - [lindex $h 3 3 0]]
set w10 [expr [lindex $h 3 3 0] - [lindex $h 6 6 0]]
set w21 [expr [lindex $h 0 0 0] - [lindex $h 1 1 0]]
set w20 [expr [lindex $h 1 1 0] - [lindex $h 2 2 0]]

```

As discussed above, simulation of lineshapes in cases where we cannot use crystallite interpolation requires a considerable number of crystallites to get a converged lineshape. Hence, instead of using the above Tcl procedure to account exchange, we have chosen to implement the same procedure in a C routine that we compile into a Tcl library through the C API of Tcl [81]. This gives the same result but with a tremendous gain in speed.

The example for a phenylalanine ring flip uses the following spin system.

```

spinsys {
  channels 2H
  nuclei 2H 2H
  quadrupole 1 1 180e3 0.05 0 60 0
  quadrupole 2 1 180e3 0.05 0 -60 0
}

```

where the only difference between the two spins is the 120° difference in their orientation corresponding to the $H^{\delta 1}$ and $H^{\delta 2}$ of phenylalanine, respectively, as explained by Vugmeyster and Ostrovsky [82]. The resulting simulations are shown for different exchange rate constants in Fig. 19B and essentially reproduce the lineshapes of Ref. [82] illustrating the versatility of SIMPSON to simulate such complex lineshapes.



8. Conclusions

We have provided a number of examples ranging from simple introductory SIMPSON simulations to advanced simulations of lineshapes under chemical exchange that serve a triple purpose: (i) provide a gentle introduction to the SIMPSON Tcl interface, (ii) to provide an introduction to various aspects of solid-state NMR, and (iii) to demonstrate the capabilities of the versatile SIMPSON interface to simulate a broad range of different pulse sequences and experiments. We believe that these examples together demonstrate that the open source software package SIMPSON may be regarded a ‘virtual NMR spectrometer’. And that with such *in silico* experiments, ultra-high fields of the currently available 1.2 GHz and above come at no extra cost.

Acknowledgements

We would like to thank for financial support from the Danish Council for Independent Research (Grant No. DFF-4090-00223) and the Danish Ministry of Higher Education and Science (Grant No. AU-2010-612-181).

References

- [1] A. Abragam, *Principles of Nuclear Magnetism*, Oxford, Clarendon Press, 1983.
- [2] O.W. Sørensen, G.W. Eich, M.H. Levitt, G. Bodenhausen, R.R. Ernst, Product operator formalism for the description of NMR pulse experiments, *Progr. Nucl. Magn. Reson. Spectrosc.* 16 (1984) 163–192.
- [3] M. Mehring, *High Resolution NMR Spectroscopy in Solids*, Springer-Verlag, Berlin Heidelberg, 1976.
- [4] R.R. Ernst, G. Bodenhausen, A. Wokaun, *Principles of Nuclear Magnetic Resonance in One and Two Dimensions*, Clarendon Press, Oxford, 1987.
- [5] A.G. Redfield, The theory of relaxation processes, *Adv. Magn. Opt. Reson.* 1 (1965) 1–32.
- [6] A. Lange, K. Giller, S. Hornig, M.F. Martin-Eauclaire, O. Pongs, S. Becker, M. Baldus, Toxin-induced conformational changes in a potassium channel revealed by solid-state NMR, *Nature* 440 (2006) 959–962.
- [7] S.D. Cady, K. Schmidt-Rohr, J. Wang, C.S. Soto, W.F. DeGrado, M. Hong, Structure of the amantadine binding site of influenza M2 proton channels in lipid bilayers, *Nature* 463 (2010) 689–692.
- [8] S.H. Park, B.B. Das, F. Casagrande, Y. Tian, H.J. Nothnagel, M. Chu, H. Kiefer, K. Maier, A.A. De Angelis, F.M. Marassi, S.J. Opella, Structure of the chemokine receptor CXCR1 in phospholipid bilayers, *Nature* 491 (2012) 779–783.
- [9] C. Wasmer, A. Lange, H. Van Melckebeke, A.B. Siemer, R. Riek, B.H. Meier, Amyloid fibrils of the HET-s(218–289) prion form a beta solenoid with a triangular hydrophobic core, *Science* 319 (2008) 1523–1526.
- [10] J.T. Nielsen, M. Bjerring, M.D. Jeppesen, R.O. Pedersen, J.M. Pedersen, K.L. Hein, T. Vosegaard, T. Skrydstrup, D.E. Otzen, N.C. Nielsen, Unique identification of supramolecular structures in amyloid fibrils by solid-state NMR spectroscopy, *Angew. Chem. Int. Ed. Engl.* 48 (2009) 2118–2121.
- [11] J.-X. Lu, W. Qiang, W.-M. Yau, C.D. Schwieters, S.C. Meredith, R. Tycko, Molecular structure of β -amyloid fibrils in Alzheimer's disease brain tissue, *Cell* 154 (2013) 1257–1268.
- [12] X. Kong, H. Deng, F. Yan, J. Kim, J.A. Swisher, B. Smit, O.M. Yaghi, J.A. Reimer, Mapping of functional groups in metal-organic frameworks, *Science* 341 (2013) 882–885.
- [13] M. Baias, J.N. Dumez, P.H. Svensson, S. Schantz, G.M. Day, L. Emsley, De novo determination of the crystal structure of a large drug molecule by crystal structure prediction-based powder NMR crystallography, *J. Am. Chem. Soc.* 135 (2013) 17501–17507.
- [14] F.S. de Bouregas, J.S. Waugh, ANTIOPE, a program for computer experiments on spin dynamics, *J. Magn. Reson.* 96 (1992) 280–289.
- [15] H. Bildsøe, STARS User's Guide. Spectrum Analysis for Rotating Solids, Publ. No. 87-195233-00, Rev. A0296, Varian Associates Inc., Palo Alto, 1996.
- [16] M. Bak, J.T. Rasmussen, N.C. Nielsen, SIMPSON: a general simulation program for solid-state NMR spectroscopy, *J. Magn. Reson.* 147 (2000) 296–330.
- [17] V. Macho, L. Brombacher, H.W. Spiess, The NMR-WEBLAB: an internet approach to NMR lineshape analysis, *Appl. Magn. Reson.* 20 (2001) 405–432.

- [18] D. Massiot, F. Fayon, M. Capron, I. King, S. Le Calvé, B. Alonso, J.-O. Durand, B. Bujoli, Z. Gan, G. Hoatson, Modelling one- and two-dimensional solid-state NMR spectra, *Magn. Reson. Chem.* 40 (2002) 70–76.
- [19] M. Veshtort, R.G. Griffin, SPINEVOLUTION: a powerful tool for the simulation of solid and liquid state NMR experiments, *J. Magn. Reson.* 178 (2006) 248–282.
- [20] M. H. Levitt, SpinDynamica NMR Calculation and Simulation in Mathematica <http://www.spindynamica.soton.ac.uk/> (accessed Jun 13, 2017).
- [21] H.J. Hogben, M. Krzystyniak, G.T.P. Charnock, P.J. Hore, I. Kuprov, Spinach—a software library for simulation of spin dynamics in large spin systems, *J. Magn. Reson.* 208 (2011) 179–194.
- [22] Z. Tosner, T. Vosegaard, C. Kehlet, N. Khaneja, S.J. Glaser, N.C. Nielsen, Optimal control in NMR spectroscopy: numerical implementation in SIMPSON, *J. Magn. Reson.* 197 (2009) 120–134.
- [23] Z. Tošner, R. Andersen, B. Stevansson, M. Edén, N.C. Nielsen, T. Vosegaard, Computer-intensive simulation of solid-state NMR experiments using SIMPSON, *J. Magn. Reson.* 246 (2014) 79–93.
- [24] Tcl Developer Site <http://www.tcl.tk/> (accessed Jun 26, 2017).
- [25] M. Bak, N.C. Nielsen, REPULSION, a novel approach to efficient powder averaging in solid-state NMR, *J. Magn. Reson.* 125 (1997) 132–139.
- [26] S.K. Zaremba, Good lattice points, discrepancy, and numerical integration, *Ann. Mat. Pur. Appl.* 73 (1966) 293–317. Series 4.
- [27] H. Conroy, Molecular Schrödinger equation. VIII. A new method for the evaluation of multidimensional integrals, *J. Chem. Phys.* 47 (1967) 5307–5318.
- [28] V.B. Cheng, H.H. Suzukawa, M. Wolfsberg, Investigations of a nonrandom numerical method for multidimensional integration, *J. Chem. Phys.* 59 (1973) 3992–3999.
- [29] S. Mamone, G. Pileio, M.H. Levitt, Orientational sampling schemes based on four dimensional polytopes, *Symmetry* 2 (2010) 1423–1449.
- [30] R. Quey, A. Villani, C. Maurice, Nearly uniform sampling of crystal orientations, *J. Appl. Cryst.* 51 (2018) 1162–1173.
- [31] D. Srivastava, T. Vosegaard, M. Dominique, P.J. Grandinetti, Core scientific dataset model: a lightweight and portable model and file format for multi-dimensional scientific data. *PLOS ONE* (2020). <https://doi.org/10.1371/journal.pone.0225953> (in press).
- [32] M. Hohwy, H. Bildsøe, H.J. Jakobsen, N.C. Nielsen, Efficient spectral simulations in NMR of rotating solids. The γ -COMPUTE algorithm, *J. Magn. Reson.* 136 (1999) 6–14.
- [33] A.E. Bennett, C.M. Rienstra, M. Auger, K.V. Lakshmi, R.G. Griffin, Heteronuclear decoupling in rotating solids, *J. Chem. Phys.* 103 (1995) 6951–6958.
- [34] A. Detken, E.H. Hardy, M. Ernst, B.H. Meier, Simple and efficient decoupling in magic-angle spinning solid-state NMR: the XiX scheme, *Chem. Phys. Lett.* 356 (2002) 298–304.
- [35] N. Sinha, C.V. Grant, C.H. Wu, A.A. De Angelis, S.C. Howell, S.J. Opella, SPINAL modulated decoupling in high field double- and triple-resonance solid-state NMR experiments on stationary samples, *J. Magn. Reson.* 177 (2005) 197–202.
- [36] K. Sharma, A. Equbal, N.C. Nielsen, P.K. Madhu, A unified heteronuclear decoupling picture in solid-state NMR under low radio-frequency amplitude and fast magic-angle-spinning frequency regime, *J. Chem. Phys.* 150 (2019) 144201.
- [37] I. Scholz, P. Hodgkinson, B.H. Meier, M. Ernst, Understanding two-pulse phase-modulated decoupling in solid-state NMR, *J. Chem. Phys.* 130 (2009) 114510.
- [38] M. Ernst, M.A. Meier, T. Tüherm, A. Samoson, B.H. Meier, Low-power high-resolution solid-state NMR of peptides and proteins, *J. Am. Chem. Soc.* 126 (2004) 4764–4765.

- [39] A. Pines, M.G. Gibby, J.S. Waugh, Proton-enhanced NMR of dilute spins in solids, *J. Chem. Phys.* 59 (1973) 569–590.
- [40] T. Gullion, J. Schaefer, Rotational-echo double-resonance NMR, *J. Magn. Reson.* 81 (1969) 196–200.
- [41] J.A. Nelder, R. Mead, A simplex method for function minimization, *Comput. J.* 7 (1965) 308–313.
- [42] Tcl libraries <http://nmr.au.dk/software/tcl-libraries/> (accessed Jul 24, 2017).
- [43] T. Vosegaard, J. Skibsted, H. Bildsøe, H.J. Jakobsen, Quadrupole coupling and anisotropic shielding from single-crystal NMR of the central transition for quadrupolar nuclei. ^{87}Rb NMR of RbClO_4 and Rb_2SO_4 , *J. Magn. Reson. A* 122 (1996) 111–119.
- [44] T.R. Field, A.D. Bain, Singularities in the lineshape of a second-order perturbed quadrupolar nucleus and their use in data fitting, *Solid State Nucl. Magn. Reson.* 61–62 (2014) 39–48.
- [45] T.R. Field, A.D. Bain, Singularities in the lineshape of a second-order perturbed quadrupolar nucleus. The magic-angle spinning case, *Solid State Nucl. Magn. Reson.* 63–64 (2014) 42–47.
- [46] B. Stevansson, M. Edén, Interpolation by fast Wigner transform for rapid calculations of magnetic resonance spectra from powders, *J. Phys. Chem.* 134 (2011) 124104.
- [47] D.W. Alderman, S. Mark, D.M.G. Solum, Methods for analyzing spectroscopic line shapes. NMR solid powder patterns, *J. Chem. Phys.* 84 (1986) 3717–3725.
- [48] L. Frydman, J.S. Harwood, Isotropic spectra of half-integer quadrupolar spins from bidimensional magic-angle spinning NMR, *J. Am. Chem. Soc.* 117 (1995) 5367–5368.
- [49] T. Vosegaard, P. Florian, D. Massiot, P.J. Grandinetti, Multiple quantum magic-angle spinning using rotary resonance excitation, *J. Chem. Phys.* 114 (2001) 4618–4624.
- [50] M. Bak, R. Schultz, T. Vosegaard, N.C. Nielsen, Specification and visualization of anisotropic interaction tensors in polypeptides and numerical simulations in biological solid-state NMR, *J. Magn. Reson.* 154 (2002) 28–45.
- [51] T. Vosegaard, A. Malmendal, N.C. Nielsen, The flexibility of SIMPSON and SIMMOL for numerical simulations in solid- and liquid-state NMR spectroscopy, *Monatsh. Chem.* 133 (2002) 1555–1574.
- [52] C.H. Wu, A. Ramamoorthy, S.J. Opella, High-resolution heteronuclear dipolar solid-state NMR spectroscopy, *J. Magn. Reson. A* 109 (1994) 270–272.
- [53] F.M. Marassi, S.J. Opella, A solid-state NMR index of helical membrane protein structure and topology, *J. Magn. Reson.* 144 (2000) 150–155.
- [54] J. Wang, J. Denny, C. Tian, S. Kim, Y. Mo, F. Kovacs, Z. Song, K. Nishimura, Z. Gan, R. Fu, J.R. Quine, T.A. Cross, Imaging membrane protein helical wheels, *J. Magn. Reson.* 144 (2000) 162–167.
- [55] F.M. Marassi, A simple approach to membrane protein secondary structure and topology based on NMR spectroscopy, *Biophys. J.* 80 (2001) 994–1003.
- [56] T. Vosegaard, N.C. Nielsen, Towards high-resolution solid-state NMR on large uniformly ^{15}N - and $^{13}\text{C},^{15}\text{N}$ -labeled membrane proteins in oriented lipid bilayers, *J. Biomol. NMR* 22 (2002) 225–247.
- [57] S. Penzel, A. Oss, M.-L. Org, A. Samoson, A. Böckmann, M. Ernst, B.H. Meier, Spinning faster: protein NMR at MAS frequencies up to 126 kHz, *J. Biomol. NMR* 73 (2019) 19–29.
- [58] L.B. Andreas, K. Jaudzems, J. Stanek, D. Lalli, A. Bertarello, T. Le Marchand, D.C.-D. Paepe, S. Kotelovica, I. Akopjana, B. Knott, S. Wegner, F. Engelke, A. Lesage, L. Emsley, K. Tars, T. Herrmann, G. Pintacuda, Structure of fully protonated proteins by proton-detected magic-angle spinning NMR, *Proc. Natl. Acad. Sci. U. S. A.* 113 (2016) 9187–9192.

- [59] A. Böckmann, M. Ernst, B.H. Meier, Spinning proteins, the faster, the better? *J. Magn. Reson.* 253 (2015) 71–79.
- [60] U. Sternberg, R. Witter, I. Kuprov, J.M. Lamley, A. Oss, J.R. Lewandowski, A. Samoson, ^1H line width dependence on MAS speed in solid state NMR—comparison of experiment and simulation, *J. Magn. Reson.* 291 (2018) 32–39.
- [61] V. Chevelkov, K. Rehbein, A. Diehl, B. Reif, Ultrahigh resolution in proton solid-state NMR spectroscopy at high levels of deuteration, *Angew. Chem. Intl. Ed.* 45 (2006) 3878–3881.
- [62] K. Xue, R. Sarkar, C. Motz, S. Asami, V. Decker, S. Wegner, Z. Tosner, B. Reif, Magic-angle spinning frequencies beyond 300 kHz are necessary to yield maximum sensitivity in selectively methyl protonated protein samples in solid-state NMR, *J. Phys. Chem. C* 122 (2018) 16437–16442.
- [63] J. Schaefer, E.O. Stejskal, J.R. Garbow, R.A. McKay, Quantitative determination of the concentrations of ^{13}C - ^{15}N chemical bonds by double cross-polarization NMR, *J. Magn. Reson.* 59 (1969) 150–156.
- [64] M. Hohwy, H.J. Jakobsen, M. Edèn, M.H. Levitt, N.C. Nielsen, Broadband dipolar recoupling in the nuclear magnetic resonance of rotating solids: a compensated C7 pulse sequence, *J. Chem. Phys.* 108 (1998) 2686–2694.
- [65] L.S. Pontryagin, *The Mathematical Theory of Optimal Processes*, New York, Interscience Publishers, 1962.
- [66] A.E. Bryson, Y.-C. Ho, *Applied Optimal Control: Optimization, Estimation, and Control*, New York, Hemisphere Publishing Corporation, 1975.
- [67] V.F. Krotov, *Global Methods in Optimal Control Theory*, Marcel Dekker, Inc., New York/Basel/Hong Kong, 1995
- [68] N. Khaneja, T. Reiss, C. Kehlet, T. Schulte-Herbrüggen, S.J. Glaser, Optimal control of coupled spin dynamics: design of NMR pulse sequences by gradient ascent algorithms, *J. Magn. Reson.* 172 (2005) 296–305.
- [69] N.C. Nielsen, C. Kehlet, S.J. Glaser, N. Khaneja, eMagRes, John Wiley & Sons, Ltd, 2007.
- [70] C.T. Kehlet, A.C. Sivertsen, M. Bjerring, T.O. Reiss, N. Khaneja, S.J. Glaser, N.C. Nielsen, Improving solid-state NMR dipolar recoupling by optimal control, *J. Am. Chem. Soc.* 126 (2004) 10202–10203.
- [71] Z. Tošner, R. Sarkar, J. Becker-Baldus, C. Glaubitz, S. Wegner, F. Engelke, S.J. Glaser, B. Reif, Overcoming volume selectivity of dipolar recoupling in biological solid-state NMR spectroscopy, *Angew. Chem. Int. Ed.* 57 (2018) 14514–14518.
- [72] T. Vosegaard, C. Kehlet, N. Khaneja, S.J. Glaser, N.C. Nielsen, Improved excitation schemes for multiple-quantum magic-angle spinning for quadrupolar nuclei designed using optimal control theory, *J. Am. Chem. Soc.* 127 (2005) 13768–13769.
- [73] C. Kehlet, T. Vosegaard, N. Khaneja, S.J. Glaser, N.C. Nielsen, Low-power homonuclear dipolar recoupling in solid-state NMR developed using optimal control theory, *Chem. Phys. Lett.* 414 (2005) 204–209.
- [74] W. Kallies, S.J. Glaser, Cooperative broadband spin echoes through optimal control, *J. Magn. Reson.* 286 (2018) 115–137.
- [75] T.E. Skinner, T.O. Reiss, B. Luy, N. Khaneja, S.J. Glaser, Application of optimal control theory to the design of broadband excitation pulses for high-resolution NMR, *J. Magn. Reson.* 163 (2003) 8–15.
- [76] D. Wei, U.Å. Akbey, B. Paaske, H. Oschkinat, B. Reif, M. Bjerring, N.C. Nielsen, Optimal ^2H rf pulses and ^2H - ^{13}C cross-polarization methods for solid-state ^2H MAS NMR of perdeuterated proteins, *J. Chem. Phys. Lett.* 2 (2011) 1289–1294.
- [77] S. Jain, M. Bjerring, N.C. Nielsen, Efficient and robust heteronuclear cross-polarization for high-speed-spinning biological solid-state NMR spectroscopy, *J. Phys. Chem. Lett.* 3 (2012) 703–708.

- [78] P. de Fouquieres, S.G. Schirmer, S.J. Glaser, I. Kuprov, Second order gradient ascent pulse engineering, *J. Magn. Reson.* 212 (2011) 412–417.
- [79] T. Vosegaard, Challenges in numerical simulations of solid-state NMR experiments: spin exchange pulse sequences, *Solid State Nucl. Magn. Reson.* 38 (2010) 77–83.
- [80] A.D. Bain, Chemical exchange in NMR, *Progr. Nucl. Magn. Reson.* 43 (2003) 63–103.
- [81] Tcl C API <https://www.tcl.tk/man/tcl8.6/TclLib/contents.htm> (accessed Dec 2, 2019).
- [82] L. Vugmeyster, D. Ostrovsky, Static solid-state ^2H NMR methods in studies of protein side-chain dynamics, *Prog. Nucl. Magn. Reson. Spectrosc.* 101 (2017) 1–17.
- [83] K. Bertelsen, B. Paaske, L. Thøgersen, E. Tajkhorshid, B. Schiott, T. Skrydstrup, N.C. Nielsen, T. Vosegaard, Residue-specific information about the dynamics of antimicrobial peptides from ^1H - ^{15}N and ^2H solid-state NMR spectroscopy, *J. Am. Chem. Soc.* 131 (2009) 18335–18342.